Plant Communications
Research article

CellPress
Partner Journal

The TELOMERE REPEAT BINDING proteins TRB4 and TRB5 function as transcriptional activators of PRC2-controlled genes to regulate plant development

Simon Amiard[1,*], Léa Feit[1], Emmanuel Vanrobays[1], Lauriane Simon[1], Samuel Le Goff[1], Loriane Loizeau[1], Léa Wolff[2], Falk Butter[3], Clara Bourbousse[2], Fredy Barneche[2], Christophe Tatout[1] and Aline V. Probst[1,*]

[1]iGReD, CNRS, Inserm, Université Clermont Auvergne, 63000 Clermont-Ferrand, France

[2]Institut de biologie de l'Ecole normale supérieure (IBENS), Ecole normale supérieure, CNRS, INSERM, Université PSL, Paris, France

[3]Institute of Molecular Biology, 55128 Mainz, Germany

***Correspondence: Simon Amiard (simon.amiard@uca.fr), Aline V. Probst (aline.probst@uca.fr)**

https://doi.org/10.1016/j.xplc.2024.100890

ABSTRACT

Plant-specific transcriptional regulators called TELOMERE REPEAT BINDING proteins (TRBs) combine two DNA-binding domains, the GH1 domain, which binds to linker DNA and is shared with H1 histones, and the Myb/SANT domain, which specifically recognizes the telobox DNA-binding site motif. TRB1, TRB2, and TRB3 proteins recruit Polycomb group complex 2 (PRC2) to deposit H3K27me3 and JMJ14 to remove H3K4me3 at gene promoters containing *telobox* motifs to repress transcription. Here, we demonstrate that TRB4 and TRB5, two related paralogs belonging to a separate TRB clade conserved in spermatophytes, regulate the transcription of several hundred genes involved in developmental responses to environmental cues. TRB4 binds to several thousand sites in the genome, mainly at transcription start sites and promoter regions of transcriptionally active and H3K4me3-marked genes, but, unlike TRB1, it is not enriched at H3K27me3-marked gene bodies. However, TRB4 can physically interact with the catalytic components of PRC2, SWINGER, and CURLY LEAF (CLF). Unexpectedly, we show that TRB4 and TRB5 are required for distinctive phenotypic traits observed in *clf* mutant plants and thus function as transcriptional activators of several hundred CLF-controlled genes, including key flowering genes. We further demonstrate that TRB4 shares multiple target genes with TRB1 and physically and genetically interacts with members of both TRB clades. Collectively, these results reveal that TRB proteins engage in both positive and negative interactions with other members of the family to regulate plant development through both PRC2-dependent and -independent mechanisms.

Key words: chromatin, TRB proteins, transcriptional regulation, PRC2, plant development

Amiard S., Feit L., Vanrobays E., Simon L., Le Goff S., Loizeau L., Wolff L., Butter F., Bourbousse C., Barneche F., Tatout C., and Probst A.V. (2024). The TELOMERE REPEAT BINDING proteins TRB4 and TRB5 function as transcriptional activators of PRC2-controlled genes to regulate plant development. Plant Comm. **5**, 100890.

INTRODUCTION

Development and adequate response to the environment require sophisticated mechanisms to precisely regulate gene expression. Conserved through evolution, the Polycomb group (PcG) proteins restrict gene activity during development by depositing repressive histone modifications, whereas proteins from the Trithorax group (TrxG) deposit histone modifications permissive for transcription and can thereby counteract the PcG machinery (Margueron and Reinberg, 2011; Schuettengruber et al., 2017). PcG function is essential for development, as loss

Published by the Plant Communications Shanghai Editorial Office in association with Cell Press, an imprint of Elsevier Inc., on behalf of CSPB and CEMPS, CAS.

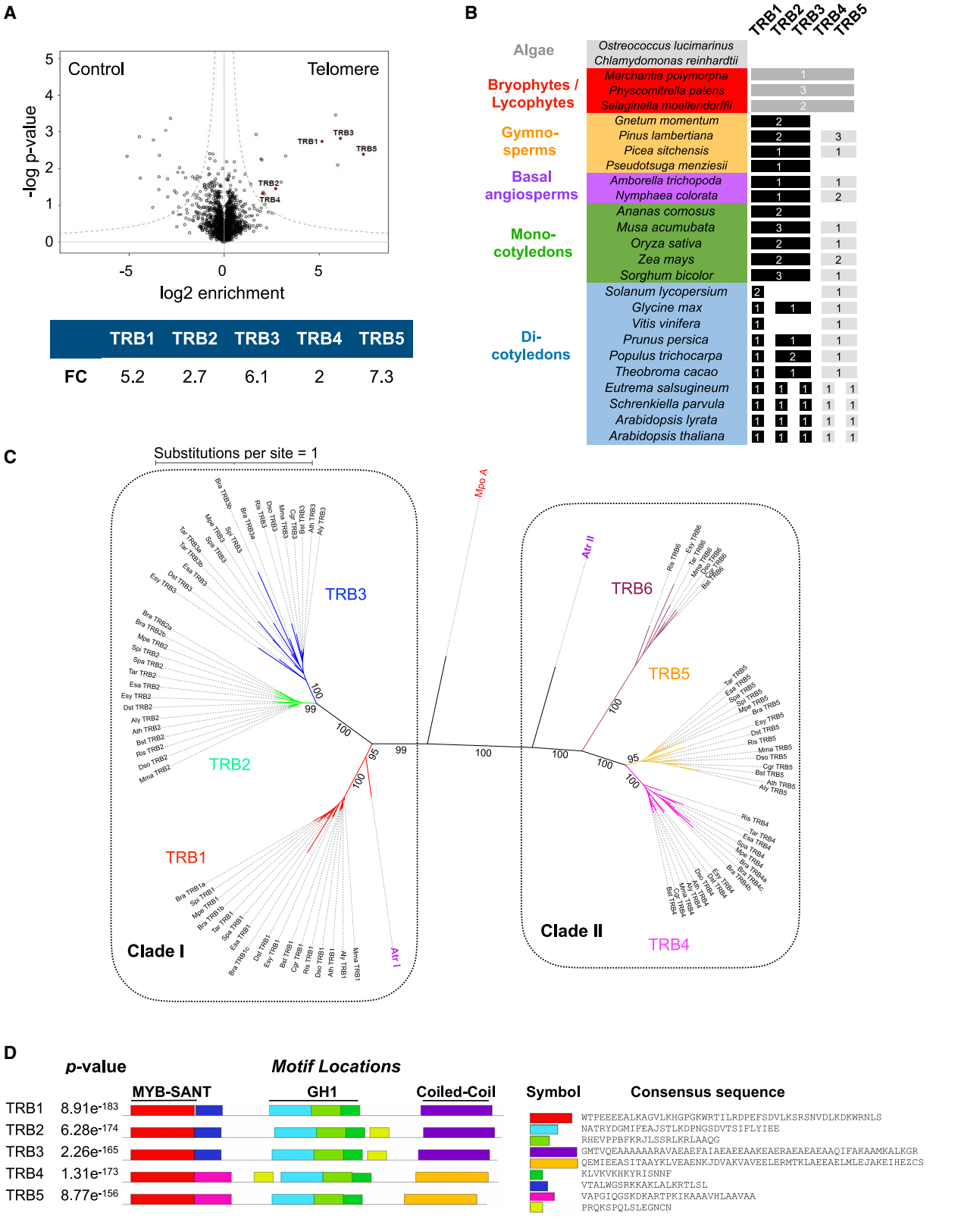

Figure 1. TRB4 and TRB5 bind to telomere repeats and belong to a separate TRB clade that is conserved in gymnosperms and angiosperms

(A) Volcano plot showing enrichment of the five TRB proteins (red dots) in the telomere repeat pull-down relative to scrambled control sequences. Mean enrichment values from four independent experiments are indicated.

(legend continued on next page)

of Polycomb activity is lethal in mice (Sauvageau and Sauvageau, 2008), causes ectopic expression of Homeotic (*Hox*) genes in *Drosophila* (Lewis, 1978), and induces severe developmental phenotypes in *Arabidopsis* (Chanvivattana et al., 2004; Bouyer et al., 2011; Simmons and Bergmann, 2016).

In animals and plants, Polycomb repressive complexes can be classified by their distinct enzymatic activities (Baile et al., 2022). Whereas PRC1 exhibits histone H2A ubiquitination activity, PRC2 complexes harbor a histone methyltransferase that trimethylates lysine 27 of histone H3 (H3K27me3). In *Drosophila*, the PRC2 complex consists of four subunits: the catalytic subunit Enhancer of zeste (E(z)), Extra sex combs (Esc), Suppressor of zeste 12 (Su(z)12), which is critical for nucleosome binding, and Nuclear remodeling factor 55 (NURF55).

In *Arabidopsis*, PRC2 complexes have undergone functional diversification with three catalytic SET-domain proteins, namely CURLY LEAF (CLF) and SWINGER (SWN), which are responsible for sporophytic H3K27me3 activity, and MEDEA (MEA), which functions in repressing endosperm proliferation, as well as three Su(z)12 orthologs termed VERNALIZATION 2 (VRN2), EMBRYONIC FLOWER 2 (EMF2), and FERTILIZATION INDEPENDENT SEED 2 (FIS2) (Simonini et al., 2021; Vijayanathan et al., 2022). This enlargement of the E(z) and Su(z)12 gene families enables assembly of several different PRC2 complexes that operate at diverse developmental stages, ensuring important developmental transitions (Wang et al., 2016). Single mutants that lack CLF, one of the possible catalytic subunits of PRC2, are viable in *Arabidopsis* but show severe developmental abnormalities (Goodrich et al., 1997). Genome-wide profiling in *Arabidopsis* identified 7000–8000 genes enriched in the H3K27me3 mark, i.e., approximately one-third of all protein-coding genes. These genes tend to be weakly expressed and to participate in development, particularly in developmental phase transitions (Zhang et al., 2007; Shu et al., 2020).

PRC2 complexes must be recruited to different target genes in a sequence-specific manner. PRC2 core subunits do not harbor intrinsic DNA-binding activity, and recruitment to target genes therefore involves associated proteins that, despite the evolutionary conservation of the PRC2 core components, differ widely among species. In *Drosophila*, PRC2 is recruited via DNA-binding proteins at Polycomb Response Elements (PREs) situated in regulatory regions of genes (Horard et al., 2000). In mammals, hypomethylated CpG islands may represent PRE-like sequences to which PRC2 can be targeted via interactions with several Transcription Factors (TFs) or non-coding RNAs (Davidovich and Cech, 2015). Binding of the Esc homolog EED to H3K27me3 methylated histones further stabilizes PRC2 and stimulates the histone methyltransferase activity of the complex (Margueron et al., 2009). PRC2 recruitment via long non-coding RNA has also been shown in plants (Ariel et al., 2014), and several *cis* elements with PRE-like characteristics have been identified and linked to PcG recruitment in *Arabidopsis*. These include a six-nucleotide RY motif (Yuan et al., 2021), the RLE element in the *LEAFY COTYLEDON 2* (*LEC2*) gene promoter (Berger et al., 2011), the ASYMMETRIC LEAVES1 (AS1) and AS2 binding sites in the *BREVIPEDICELLUS* and *KNAT2* promoters (Lodha et al., 2013), and the GAGA and telobox (Deng et al., 2013; Zhou et al., 2016; Xiao et al., 2017), short motifs abundant in gene promoters that in turn are bound by specific proteins that recruit the Polycomb complexes.

One group of such plant-specific proteins that preferentially bind to telomeric motifs (so-called teloboxes) via their Myb-like DNA-binding domain is the TELOMERE REPEAT BINDING (TRB) protein family, which consists of five members (TRB1–5) in *Arabidopsis* (Schrumpfova et al., 2004; Schrumpfová et al., 2014). TRB1, TRB2, and TRB3 were initially shown to bind telomeres consisting of long tandem repeats of teloboxes and were proposed to function in telomere protection (Schrumpfova et al., 2004; Mozgová et al., 2008). In addition to the N-terminal Myb-domain, TRB proteins contain a second DNA-binding domain, the globular H1 (GH1) domain, shared with linker histone H1, which mediates binding to the nucleosome dyad and linker DNA (Bednar et al., 2017). The GH1 domain is also involved in TRB protein–protein interactions, including TRB1 homodimerization (Mozgová et al., 2008) and heterodimerization with TRB2 and TRB3 (Schrumpfová et al., 2008). TRB1–3 proteins finally contain a coiled-coil region in their C termini that interacts with the catalytic PRC2 subunits CLF and SWN, triggering H3K27me3 deposition at a subset of PRC2 target genes (Zhou et al., 2016, 2018). This role in gene repression is further reinforced by the interaction of TRB1, TRB2, and TRB3 with the JMJ14 H3K4me3 demethylase, which both counteracts the maintenance of a transcriptionally permissive state and establishes a repressive chromatin state (Wang et al., 2023). Recruitment of PRC2 activity mediated by TRB1–3-is restricted by specific chromatin characteristics such as the presence of linker histone H1: in the absence of H1, TRB1 accumulates at telomeres and interstitial telomere repeat sequences within the pericentromeric regions of specific chromosomes, leading to accumulation of H3K27me3 at these sequences (Teano et al., 2023). In addition to its function in PRC2 targeting, TRB1 has also been shown to maintain high expression levels of genes involved in metabolic processes, such as photosynthesis (Zhou et al., 2016), revealing an as-yet poorly understood mode of action that may depend on target genes, other transcriptional regulators, and chromatin context. Finally, TRB1 and TRB2 are also members of the PEAT (PWWPs–EPCRs–ARIDs–TRBs) complex, which is required for histone deacetylation at transposable elements (TEs) and heterochromatin silencing (Tan et al., 2018).

(B) Presence or absence of orthologs of the *Arabidopsis* TRB proteins in different plant species spanning the evolutionary history of land plants. TRB orthologs were detected in the liverwort *Marchantia,* and orthologs of TRB1–3 (black) and TRB4–5 (gray) are present in gymnosperms, basal angiosperms, and mono- and dicotyledons.

(C) Unrooted maximum-likelihood phylogenetic tree of 87 TRB orthologs from 15 Brassicaceae species.

(D) Presentation of nine motifs in the *A. thaliana* TRB proteins predicted with MEME from an alignment of TRB orthologs from 15 Brassicaceae species. Sequences of consensus motifs are indicated. Distinct motifs adjacent to the MYB/SANT domain and different coiled-coil domains in the C termini differentiate clade I from clade II TRB proteins.

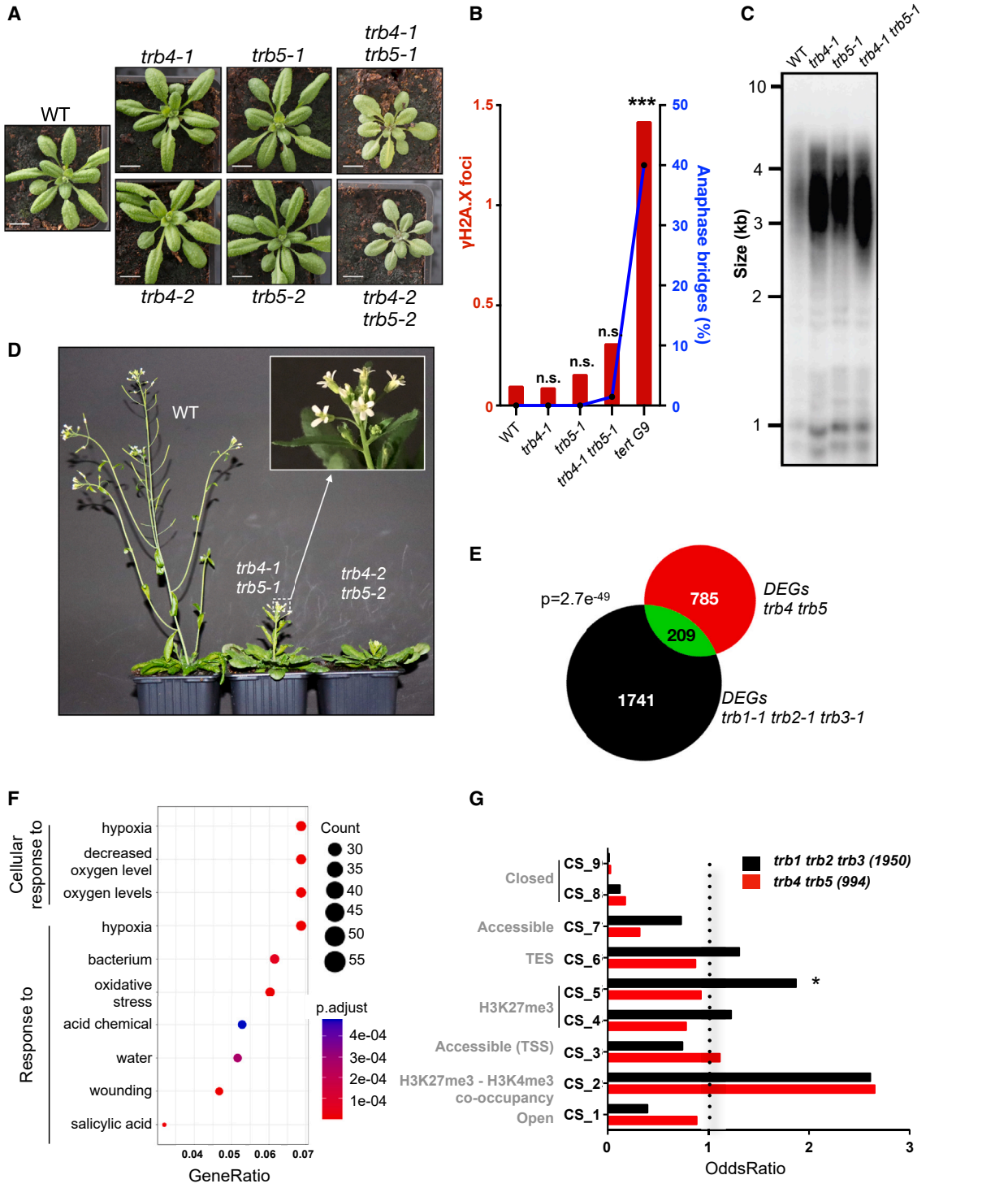

Figure 2. TRB4 and TRB5 are transcriptional regulators required for plant development but not for telomere protection

(A) Representative WT, *trb4-1*, *trb5-1*, *trb4-2*, and *trb5-2* single- and double-mutant plants at 3 weeks of age.

(B) Percentage of anaphase bridges (blue line) and mean number of γH2A.X foci (histogram, red) in the WT, *trb4-1* and *trb5-1* single mutants, and *trb4-1 trb5-1* double mutants. Plants lacking the telomerase reverse transcriptase TERT in the 9th generation (*tert G9*) (Fitzgerald et al., 1999) were used as a positive control of telomere deprotection. For anaphase bridges, the mean percentage of bridges observed in 100 mitoses from five individual plants and, for γH2A.X foci, the mean number of foci in 100 nuclei isolated from five individual plants from each genotype are indicated (***$p < 0.0001$, *t-test*).

(C) TRF analysis of bulk telomere length in genomic DNA using telomere repeat probes in the WT, *trb4-1* and *trb5-1* single mutants, and *trb4-1 trb5-1* double mutants.

(legend continued on next page)

TRB1, TRB2, and TRB3 seem to fulfill redundant roles in *Arabidopsis*, as phenotypes of the single and double mutants are indistinguishable from those of wild-type (WT) plants. Triple *trb1 trb2 trb3* mutants, however, exhibit strong developmental defects like those observed in mutants that lack PRC2 complex activity (Zhou et al., 2018). Although several functions of TRB1–3 have been characterized, it remains unclear whether and how other TRB family members contribute to gene expression regulation and plant development.

Here, we demonstrate that *Arabidopsis* TRB4 and TRB5, which diverged into a distinct clade from Brassicaceae TRB1–3 at the time of the appearance of seed plants (Kusová et al., 2023), are nuclear proteins that redundantly regulate development. Genome-wide profiling revealed that TRB4 associates with both unique and TRB1-shared target genes, consistent with the observation that all TRB proteins engage in homo- and heterodimerization. Whereas TRB1 accumulates at the gene bodies of only a subset of H3K27me3-enriched genes, TRB4 preferentially binds to transcription start sites and promoter regions of H3K4me3-enriched and transcriptionally active genes. Notably, genes that are misregulated in *trb4 trb5* double-mutant plants are overrepresented among genes that show co-occurrence of H3K4me3 and H3K27me3. However, even though TRB4 physically interacts with PRC2 subunits, the absence of TRB4 and TRB5 only affects the enrichment of H3K27me3 and H3K4me3 at a small subset of genes. This implies that TRB4 and TRB5 function independently of these histone marks. Finally, we reveal that TRB4 and TRB5 are unexpectedly required for the early-flowering and leaf-curling phenotype of mutants that lack the catalytic subunit CLF, likely owing to their roles as positive transcriptional regulators of CLF-controlled genes, including key flowering regulators like *FT*, as well as MADS-box genes such as *SEP1–3* and *SOC1*. We suggest that TRB4 and TRB5 proteins fine-tune gene expression during development in both a PcG-dependent and -independent manner, in concert with the other members of the TRB family.

RESULTS

TRB4 and TRB5 proteins belong to a separate phylogenetic clade

In an initial attempt to identify proteins with the capacity to bind telomere repeats, we performed a label-free quantitative proteomics analysis of proteins binding to the *Arabidopsis* TTTAGGG repeat sequence (Charbonnel et al., 2018). In addition to TRB1, TRB2, and TRB3, data re-analysis identified two poorly characterized members of the TRB family, namely TRB4 and TRB5, which were significantly enriched (fold change [FC] of 2 and 7.3, respectively) in the telomere pull-down compared with the shuffled DNA control (Figure 1A). Previous studies suggested that TRB4 and TRB5 belong to a separate clade in the TRB phylogeny (Kotlinski et al., 2017; Kusová et al., 2023). To time the appearance of this clade, we selected 24 species to represent the diversity of the green land-plant lineage and interrogated several databases using *Arabidopsis* TRB1–TRB5 as queries. TRB orthologs were not found in unicellular algae, but a parental TRB protein containing both an amino-terminal Myb/SANT domain and a central GH1 domain was present in bryophytes and had undergone duplication and diversification in an ancestral species of spermatophytes (Figure 1B; Supplemental Table 1). Phylogenetic analysis using IQ-Tree (Supplemental Figure 1A) identified two separate TRB clades conserved in both gymnosperms and angiosperms that contained *Arabidopsis* TRB1–3 or TRB4–5 and which we termed clade I and clade II, respectively. Longer branch lengths were observed for clade II than for clade I (0.27 versus 0.39 substitutions per site per species in clade I and clade II, respectively; $p < 0.0062$), indicating higher evolutionary divergence in clade II. Within each clade, TRB proteins of gymnosperms, monocotyledons, and dicotyledons were grouped together. In dicotyledons, *TRB* genes had undergone expansion and sub-functionalization. For example, in clade I, TRB proteins had diverged from a common ancestor into a TRB1 subclade and a TRB2/3 subclade. We also noticed that TRB1 and TRB4/5 orthologs were present in all dicotyledons, whereas representatives of the TRB2/3 sub-clade were absent from certain species (Figure 1B).

Because TRB proteins had diversified even further within the Brassicaceae, we analyzed in more detail the phylogenetic relationships of 87 TRB orthologs from 15 species of this family in more detail (Figure 1C). An unrooted phylogenetic tree confirmed that, within clade I, the TRB1 and TRB2/3 subclades resulted from duplication of a common ancestor gene and that TRB2 and TRB3 on the one hand, and TRB4 and TRB5 on the other, diverged after more recent duplications from ancestors within each subclade (Figure 1C). Finally, seven of the 15 analyzed Brassicaceae species encoded proteins that were grouped into an additional TRB subclade of clade II TRBs, which we termed TRB6 (Figure 1C).

Using all TRB orthologs from the Brassicaceae family as input, we then predicted protein motifs (Figure 1D; Supplemental Figure 1B). MEME analysis revealed clade-specific motifs adjacent to the Myb/SANT domain and in the C-terminal portion of the TRB proteins (Figure 1D). The latter were identified by InterProScan as coiled-coil domains and were predicted by AlphaFold (Jumper et al., 2021) to form long α helices (Supplemental Figure 1C). Most TRB1 proteins also contained a supplementary motif specific to TRB1 orthologs (Supplemental Figure 1B). Finally, a short motif present between the GH1 and the coiled-coil domain in most clade I TRB proteins

(D) Representative single- and double-mutant plants at the flowering stage. Double mutants show delayed flowering and supernumerary petals (quantification in Supplemental Figure 2H and 2I).

(E) Venn diagram showing numbers of DEGs in *trb4 trb5* and *trb1 trb2 trb3* mutants and those common to both mutant combinations. Significance of common DEGs was determined using a hypergeometric test.

(F) GO-term enrichment of *trb4 trb5* DEGs defined using ClusterProfiler.

(G) Enrichment of *trb4 trb5* and *trb1 trb2 trb3* DEGs in the nine CSs defined by Sequeira-Mendes et al. (2014) (*odds ratio [OR] >1 and $p < 0.05$).

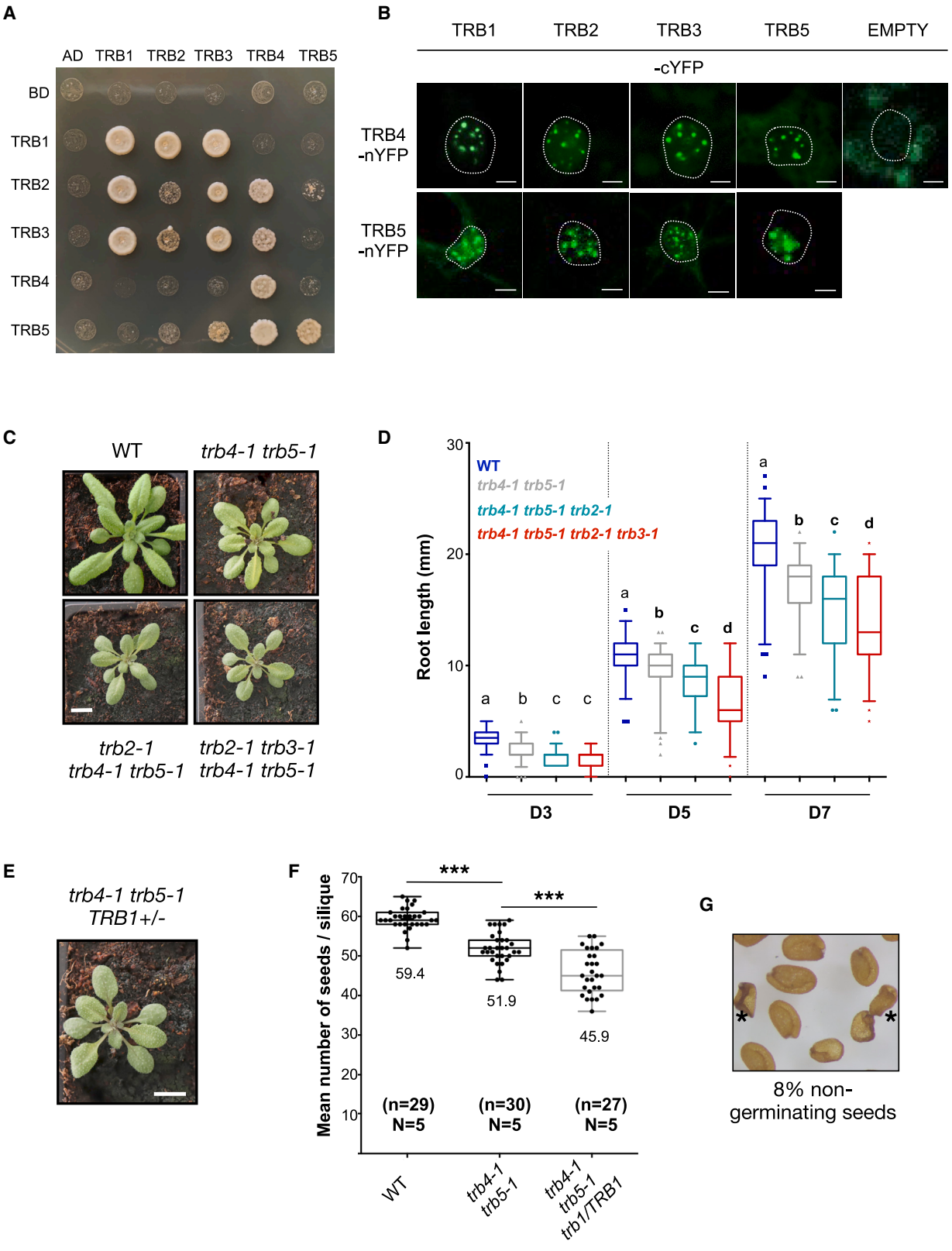

Figure 3. TRB proteins from the two clades physically and genetically interact with each other.

(A) Interactions among the five *Arabidopsis* TRB proteins probed in the Y2H system. Growth on selective medium lacking histidine and adenine reveals interaction between the two proteins tested. Horizontal, translational fusions with the Gal4-Activation domain (AD); vertical, translational fusion with the Gal4-DNA-binding domain (BD). BD and AD indicate the respective empty vectors.

(legend continued on next page)

(Supplemental Figure 1B) was also found in TRB4, although at a different position in the protein, suggesting genomic rearrangements.

In summary, TRB4 and TRB5 share the two DNA-binding domains with TRB1–3. Nevertheless, the TRB proteins were clearly separated into two phylogenetic clades distinguished by divergent regions, in particular the coiled-coil C-terminal region involved in protein–protein interactions between TRB1–3 and the PRC2 complex (Zhou et al., 2018), thus suggesting the possibility of functional diversification of the clade II TRB proteins.

TRB4 and TRB5 fine-tune plant development and gene expression but are dispensable for telomere protection

Given their interaction with telomere repeats, we first investigated whether TRB4 and TRB5 play a role in telomere regulation or stability. We generated CRISPR-Cas9 loss-of-function alleles by targeting Cas9 to the first exon of *TRB4* and the second exon of *TRB5*. For each gene, we retained two independent mutant alleles in which nucleotide insertions or deletions led to frameshifts that resulted in premature stop codons (Supplemental Figure 2A). All mutants were therefore expected to be null mutants. *TRB4* or *TRB5* loss-of function plants did not show any developmental abnormalities (Figure 2A) or alterations in telomere maintenance, as determined by quantifying the number of anaphase bridges in inflorescences and γH2A.X foci in root-tip nuclei (Figure 2B) or by testing potential telomere deprotection using telomere restriction fragment (TRF) analysis of bulk telomere length (Figure 2C and Supplemental Figure 2B–2D). Because *TRB4* and *TRB5* might be functionally redundant, we generated *trb4 trb5* double mutants that also showed no defects in telomere maintenance (Figure 2B and 2C). Hence, although these two proteins target telomeric DNA, their removal is not sufficient for telomere deprotection.

Nevertheless, we noticed several important developmental abnormalities in the *trb4 trb5* double mutants: young seedlings were smaller compared with WT plants or single mutants and showed brighter leaf color and shorter roots (Figure 2A; Supplemental Figure 2E). Adult plants displayed delayed flowering and reduced fertility (Figure 2D; Supplemental Figure 2F–2H). Furthermore, ∼30% of *trb4-1 trb5-1* double-mutant flowers harbored supernumerary petals (Figure 2D (inset), Supplemental Figure 2I), a phenotype previously observed in mutants for histone H3K27 demethylases (Yan et al., 2018) and TrxG (Carles et al., 2005). Hence, complementation of the *trb4-1 trb5-1* mutant with either *TRB4* or *TRB5* expressed under the control of their respective endogenous promoters fully restored the WT phenotype, confirming that TRB4 and TRB5 have redundant functions (Supplemental Figure 2G–2I).

To address how TRB4 and TRB5 affect plant development, we analyzed the transcriptome of 7-day-old seedlings of the WT, two independent *trb4 trb5* double-mutant lines, and a *trb1-1 trb2-1 trb3-1* triple-mutant line by RNA sequencing (RNA-seq). We retained 994 differentially expressed genes (DEGs), 62% (618) upregulated and 38% (376) downregulated, shared among mutant plants combining distinct *trb4 trb5* mutant alleles (Supplemental Figure 2J). More than half of the misregulated genes were categorized as functioning in response to stress and were linked to cellular responses to hypoxia, oxygen, light, and hormone levels (Figure 2F), implying that the plant's response to environmental stimuli is affected by loss of TRB4 and TRB5. Because one of the most prominent Gene Ontology (GO) terms was cellular response to hypoxia, we exposed WT and mutant plants to hydrogen peroxide. Root growth of *trb4-1 trb5-1* mutant plants was slightly more sensitive to hydrogen peroxide than that of the WT, suggesting a role for TRB4 and TRB5 in the transcriptional response to redox stress (Supplemental Figure 2K). In addition to genes involved in cellular responses to environmental stress, several genes encoding TFs from the AP2/ERF, homeobox, and MADS-box transcription factor families were also misregulated, including the flowering regulator genes *SUPPRESSOR OF OVEREXPRESSION OF CO 1* (*SOC1*) and *FLOWERING LOCUS C* (*FLC*) (Supplemental Table 2; Supplemental Figure 2L). Because *soc1* mutant plants display delayed flowering (Samach et al., 2000) and FLC is a flowering repressor (Michaels and Amasino, 1999), *SOC1* downregulation and *FLC* upregulation in *trb4 trb5* plants could at least partly explain the late-flowering phenotype of the *trb4 trb5* mutant.

The number of DEGs in *trb4 trb5* plants was lower (n = 994) than the number of DEGs in *trb1-1 trb2-1 trb3-1* triple mutants (n = 1950) shared between our dataset and a previous one (Zhou et al., 2018) (Figure 2E, Supplemental Figure 2J and 2M), consistent with the milder developmental phenotype of these plant lines. However, *trb4 trb5* plants shared 21% of their DEGs with *trb1 trb2 trb3* triple mutants, both oppositely and co-regulated (Supplemental Figure 2N), showing that subsets of

(B) BiFC reveals protein–protein interactions (PPIs) between TRB proteins within each clade and between proteins from the TRB_I and TRB_II clades in *N. benthamiana* leaf cells. Maximum intensity projections of z stacks acquired with a confocal microscope are shown. PPI takes place within distinct nuclear speckles, which likely correspond to telomeres. No signal was observed when TRB4-nYFP was co-expressed with the C-terminal part of YFP alone.

(C) Representative WT, *trb4-1 trb5-1* double-mutant, *trb2-1 trb4-1 trb5-1* triple-mutant, and *trb2-1 trb3-1 trb4-1 trb5-1* quadruple-mutant plants at 3 weeks of age. Scale bar, 1 cm.

(D) Quantification of the root length of *in vitro*-grown WT, *trb4-1 trb5-1* double mutants, *trb2-1 trb4-1 trb5-1* triple mutants, and *trb2-1 trb3-1 trb4-1 trb5-1* quadruple mutants at days 3 (D3), 5 (D5), and 7 (D7) after germination. For each time point, values from two independent replicates are shown. Different letters indicate significant differences determined by Mann–Whitney test ($p < 0.01$) among samples from the same time point.

(E) Representative *trb4-1 trb5-1 trb1-1/TRB1* mutant plant. Scale bar, 1 cm.

(F) Mean number of seeds per silique from WT, *trb4-1 trb5-1*, and *trb4-1 trb5-1 trb1-1/TRB1* plants. Seeds from at least 27 siliques from five plants were counted. About 12% fewer seeds were present in the *trb4-1 trb5-1* mother plant heterozygous for the *trb1* mutation compared with the *trb4-1 trb5-1* double mutants (***$p < 0.0001$, *t-test*).

(G) Seeds from *trb4-1 trb5-1 trb1-1/TRB1* plants, revealing the presence of shriveled, non-germinating seeds marked with an asterisk.

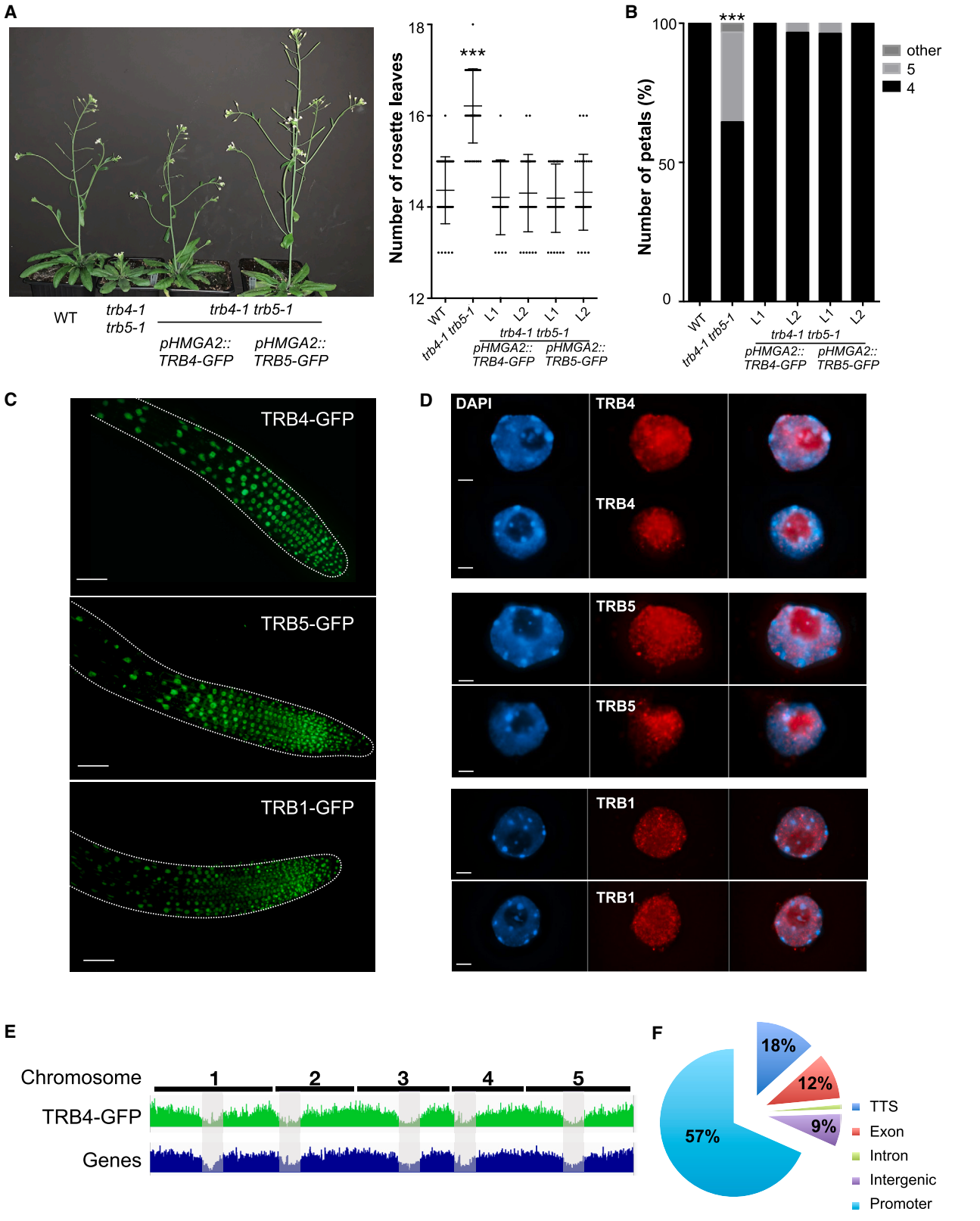

Figure 4. TRB4 and TRB5 are nuclear proteins enriched in euchromatin, and TRB4 preferentially binds to gene promoters

TRB4-GFP or TRB5-GFP fusion proteins expressed under the *GH1-HMGA2* promoter complemented the late-flowering and supernumerary-petal phenotype of *trb4-1 trb5-1* double mutants.

(legend continued on next page)

genes are directly or indirectly regulated by members of both TRB clades. To explore whether loss of TRB4 and TRB5 preferentially affects genes with a particular chromatin state (CS), we analyzed whether the TSSs of the misregulated genes were characterized by any of the previously identified CSs (Sequeira-Mendes et al., 2014) (Figure 2G). Consistent with the involvement of TRB1–3 in PcG-mediated transcriptional control, genes differentially regulated in *trb1 trb2 trb3* were overrepresented among genes corresponding to CS5 (H3K27me3-rich) and genes showing co-occurrence of both H3K4me3 and H3K27me3 modifications (CS2) (Sequeira-Mendes et al., 2014). By contrast, *trb4 trb5* DEGs were mainly overrepresented among genes associated with CS2 but not with CS5. Whereas TRB1–3 proteins are involved in TE silencing as part of the PEAT complex (Tan et al., 2018), we did not observe a strong reactivation of TEs in *trb4 trb5* mutant plants (17 TEs up, 13 TEs down), revealing that the primary function of TRB4–5 proteins is the control of gene expression.

TRB proteins of the two clades physically and genetically interact with each other

Clade I TRB proteins were previously shown to interact with each other through their GH1 domain (Schrumpfová et al., 2008). We therefore speculated that similar interactions might take place within clade II (TRB4–5) or between the two clades. To test this possibility, we carried out yeast two-hybrid (Y2H) experiments using each protein as either bait or prey. Our assay confirmed known interactions among clade I members and, in agreement with Kusová et al. (2023), showed that TRB4 and TRB5 can homo- and heterodimerize in yeast (Figure 3A; Supplemental Figure 3A). We further observed that TRB4 interacted with TRB2 and TRB3, indicating that interactions can take place between TRB proteins from different clades. To test the occurrence of these interactions *in planta*, we used bimolecular fluorescence complementation (BiFC) assays in *Nicotiana benthamiana* leaves. BiFC confirmed the protein–protein interactions identified by Y2H and revealed additional interactions between TRB1 and TRB4, as well as between TRB5 and TRB1–3 (Figure 3B). Protein–protein interactions between the different TRB clades all took place in the nucleus and were concentrated in a few bright nuclear speckles, likely corresponding to *N. benthamiana* telomeres, as observed in (Schrumpfová et al., 2014).

Given the physical interactions between the different TRB proteins, we explored their genetic interactions in multiple mutants obtained by first crossing *trb1-1*, *trb2-1*, or *trb3-1* single mutants with *trb4-1 trb5-1* plants and then performing crosses of the resulting multiple mutants. From the segregating populations, we obtained viable *trb2-1 trb4-1 trb5-1* triple-mutant plants and *trb2-1 trb3-1 trb4-1 trb5-1* quadruple-mutant plants, which strongly resembled clade II *trb* mutants but showed more pronounced developmental deficiencies, including smaller rosettes (Figure 3C) and aggravated root growth defects (Figure 3D).

By contrast, all attempts to obtain *trb1-1 trb4-1 trb5-1* triple mutants failed. Closer inspection of the siliques from *trb1-1/TRB1 trb4-1 trb5-1* plants (Figure 3E) revealed aborted ovules and a smaller number of seeds per silique (Figure 3F), indicating failed fertilization or early abortion of the developing seeds. However, less than 25% of the ovules aborted, suggesting that a fraction of triple mutants completed seed development. Indeed, 8% (41 out of 509) of the seeds failed to germinate (Figure 3G), so all surviving plantlets were either WT or heterozygous for the *trb1* mutation (65% *TRB1/trb1* and 35% *TRB1/TRB1*, $n = 89$). In the absence of clade II TRB proteins, TRB1 therefore fulfills an essential function that cannot be complemented by TRB2 or TRB3. The requirement for TRB1 in the *trb4 trb5* mutant background might be explained by its higher expression in the embryo and endosperm (Supplemental Figure 3C) or by an as-yet undefined specific role of TRB1, the only clade I TRB protein present in all dicotyledonous species analyzed (Figure 1B, left).

TRB4 binds preferentially to promoter regions

To study the localization of TRB4 and TRB5, we expressed both proteins as translational fusions with GFP. As estimated from a full restoration of WT flowering time and normal petal development in the *trb4-1 trb5-1* double-mutant background, these TRB4-GFP and TRB5-GFP fusion proteins were functional (Figure 4A and 4B). We first imaged GFP fluorescence in root tips of young plantlets and found that TRB4 and TRB5 localized in the nucleus (Figure 4C), as previously observed for TRB1, TRB2, and TRB3 (Schrumpfová et al., 2014; Zhou et al., 2018) and confirmed here for TRB1 (Figure 4C). Making use of these transgenic plants, we performed immunofluorescence staining of isolated nuclei from 7-day-old seedlings to examine the subnuclear localization of TRB1, TRB4, and TRB5 in more detail. The three proteins localized throughout the euchromatin, sometimes as small speckles, but were depleted from the DAPI-bright heterochromatic chromocenters (Figure 4D). TRB4 and TRB5, as well as TRB1, were also detected in the nucleolus, as previously observed after transient expression of TRBs in *N. benthamiana* leaves (Zhou et al., 2016; Kusová et al., 2023). To obtain a precise view of the genomic distribution of clade II TRB proteins, we carried out chromatin immunoprecipitation sequencing (ChIP-seq) targeting TRB4-GFP in 7-day-old plantlets and identified more than 5000 TRB4 peaks that were robustly detected in two independent biological replicates (Supplemental Figure 4A). Consistent with our microscopy

(A) Representative 4-week-old plants (left). Quantification (right) of the number of leaves at bolting in WT, *trb4-1 trb5-1* double mutants, and four independent transgenic lines expressing TRB4-GFP or TRB5-GFP. ***$p < 0.0001$, *t-test*.
(B) Percentage of flowers with four, five, or any other aberrant number of petals in the same genotypes as in **(A)**. ***$p < 0.001$, *t-test*.
(C) Representative root tips of plants expressing TRB4, TRB5, or TRB1 as a GFP fusion. Fusion proteins were localized in the nucleus. Scale bar, 50 μm.
(D) Maximum intensity projections of nuclei from plantlets expressing TRB4, TRB5, or TRB1 as a GFP fusion; fusion proteins were revealed by immunofluorescence staining with an anti-GFP antibody (red). TRB4, TRB5, and TRB1 localized to small discrete speckles throughout the euchromatin. DNA was counterstained with DAPI (blue, left). Merged images are shown on the right. Scale bar, 2 μm.
(E) Comparison of the distribution of TRB4-GFP ChIP-seq peaks and genes along the five *Arabidopsis* chromosomes. Gray zones indicate centromeric and pericentromeric regions.
(F) Distribution of TRB4 peaks among different genomic features in the *Arabidopsis* genome as determined by ChIP-seq.

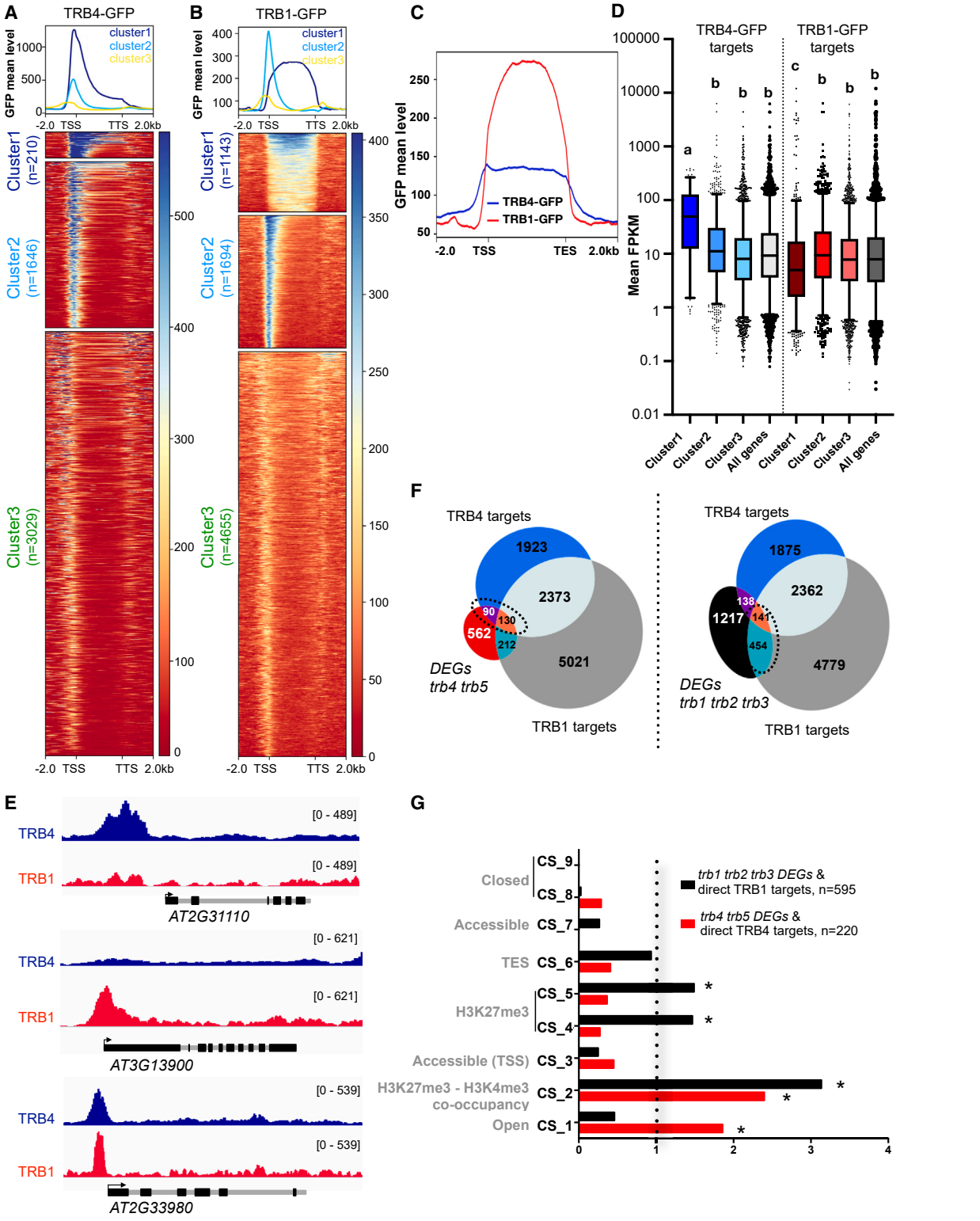

Figure 5. TRB1 and TRB4 are differentially distributed along the genome but share target genes

(A and B) Metagene plots and heatmaps after k-means clustering showing ChIP-seq signals of TRB4-GFP **(A)** and TRB1-GFP **(B)** over TRB4 and TRB1 target genes, respectively.

(C) Metagene plot showing enrichment of TRB1-GFP and TRB4-GFP over TRB1 cluster 1 genes (n = 1143).

(D) Mean expression (FPKM) of genes within the three clusters and for all TRB4-GFP or TRB1-GFP target genes. Different letters indicate significant differences among samples determined by *t-test* ($p < 0.01$).

(legend continued on next page)

observations, TRB4-GFP-associated loci were enriched at chromosome arms and depleted from pericentromeric heterochromatic regions (Figure 4E). Over 68% of the TRB4 peaks were situated in gene promoters (Figure 4F). As reported for TRB1 (Schrumpfová et al., 2015; Zhou et al., 2016; Teano et al., 2023), *de novo motif discovery identified* the telobox consensus motif (*TAGGGTT*) as the most enriched motif, present at about 49% of TRB4 genomic binding sites (MEME, $p = 7.4^{e-32}$). TRB4-GFP was also significantly enriched at loci bearing the site II motif (*TGGGCY*), which is typically associated with the telobox motif in promoters of ribosomal genes (Gaspin et al., 2010) (Supplemental Figure 4B). Thus, TRB4 binds preferentially to promoters and TSSs, many of which carry telobox motifs, although TRB4 is also present at telobox-free sites through a recruitment mode that remains to be discovered.

TRB4 and TRB1 show different binding patterns along genes but share targets and engage in complex gene co-regulation

To obtain a detailed view of differences in TRB1 and TRB4 binding, we performed k-means clustering of their target genes (Figure 5A). In cluster 1 and 2, TRB4 strongly marked the TSS, whereas cluster 3 contained genes that showed TRB4 binding further upstream and/or downstream of the TSS. Motif analyses of the 5′ UTRs of cluster 1 and 2 genes indicated a strong enrichment (E-value > 1^{e-200}) in telobox motifs, whereas no significant enrichment of this motif was found in the promoters and 5′ UTRs (−1000 bp) of genes from cluster 3 (Supplemental Figure 5). Genes in cluster 1 showed significantly higher expression than the average of all TRB4 target genes or those in cluster 2 and 3 (Figure 5D). As observed for TRB4, k-means clustering of the TRB1 binding sites identified in our recent study (Teano et al., 2023) revealed a group with enrichment at the TSS (TRB1 cluster 2), similar to TRB4 clusters 1 and 2 (Figure 5B). By contrast, TRB1 cluster 1 comprised a group of genes for which TRB1 marked the entire gene body and for which no telobox motif enrichment was found in the 5′ UTR or coding sequence (Supplemental Figure 5). Plotting TRB1 and TRB4 on TRB1 cluster 1 genes indicated that, with the exception of several genes, these genes were preferentially enriched in TRB1 but not in TRB4 (Figure 5C). Interestingly, genes targeted by TRB4 or TRB1 at their TSSs (TRB4 clusters 1 and 2, TRB1 cluster 2) were frequently involved in ribosome biogenesis and translation, consistent with the enrichment of telobox and site II motifs in their promoters, whereas genes in which TRB1 bound to the gene body (TRB1 cluster 1) were frequently involved in stress and developmental responses (Supplemental Figure 5). Plotting the mean gene expression levels for each cluster showed that TRB1 specifically targets a group of low-expressed genes in their gene bodies (cluster 1), whereas TRB4 targets a group of genes that are particularly highly expressed (Figure 5D), illustrating specialization among the members of the different TRB clades.

Given the ability of TRB1 and TRB4 proteins to form heterodimers (Kusová et al., 2023; Figure 3A and 3B) and to bind to similar consensus sequences, we searched for potential TRB1 and TRB4 co-occurrence. In addition to TRB1- and TRB4-specific target sites, TRB4 shared more than half of its binding sites with TRB1 (Figure 5E and 5F). Comparison of the TRB1 and TRB4 targets identified by ChIP-seq with the list of genes misregulated in *trb4 trb5* or *trb1 trb2 trb3* mutant lines identified a few hundred genes plausibly directly regulated by TRB1 or TRB4 (Figure 5F). Half of the misregulated genes that were directly targeted by TRB4 ($n = 220$) were upregulated, whereas the other half were downregulated, suggesting that TRB4 can act as either a positive or negative regulator of transcription, possibly depending on the genomic context or on specific protein interactions. Comparison of *trb4 trb5* mutant DEGs with TRB1 targets also revealed a small but significant number of genes that were either commonly targeted by TRB4 and TRB1 ($n = 130$) or specifically targeted by TRB1 ($n = 212$) or TRB4 ($n = 90$) (Figure 5E and 5F). These observations suggest the existence of distinct TRB complexes in which TRB1 and TRB4 often bind to common genes and potentially influence each other's function to regulate gene expression.

TRB4 is enriched at H3K4me3-marked genes but does not affect H3K4me3 deposition

Closer investigation of the CSs associated with genes misregulated in the *trb1 trb2 trb3* or *trb4 trb5* mutant plants and directly bound by either TRB1 or TRB4 revealed that TRB1 targets were overrepresented among genes corresponding to the reference CS2, CS4, and CS5 CSs, which are enriched in H3K27me3 and consist mainly of silent or low-expressed genes in public datasets (Sequeira-Mendes et al., 2014) (Figure 5G). Instead, TRB4-associated genes are overrepresented among genes that carry both H3K27me3 and H3K4me3 (CS2) or CS1, which usually encompasses active genes with strong H3K4me3 enrichment (Figure 5G).

To gain insight into the chromatin marks present at TRB4 and TRB1 binding sites, we carried out H3K4me3 and H3K27me3 ChIP-seq at the same developmental stage (i.e., in 7-day-old seedlings) and plotted the distribution of TRB4 and TRB1 as a function of the presence and/or absence of these post-translational modifications. Our ChIP-seq profiles showed that although TRB1 was associated with the bodies of genes marked by H3K27me3 or by both H3K4me3 and H3K27me3, as expected, TRB4 was excluded from H3K27me3-marked gene bodies but moderately enriched at TSSs and TTSs (Figure 6A).

Although TRB1-GFP and TRB4-GFP mean profiles at genes differed, with TRB4-GFP typically enriched at the 5′ and 3′ ends

(E) Genome Browser views of representative genes that are targets of TRB4, TRB1, or both.

(F) Venn diagrams showing the overlap between TRB1 (gray) and TRB4 (blue) targets and DEGs in *trb4 trb5* (left) or *trb1 trb2 trb3* mutants (right). Overlap TRB4 targets/TRB1 targets ($n = 2503$), $p = 0$; DEGs *trb4 trb5*/TRB4 targets ($n = 220$), $p = 3.6e^{-09}$; DEGs *trb1 trb2 trb3*/TRB1 targets ($n = 595$), $p = 9.4e^{-06}$; DEGs *trb4 trb5*/TRB1 targets ($n = 342$), $p = 5.6e^{-09}$; and DEGs *trb1 trb2 trb3*/TRB4 targets ($n = 279$), $p = 0.98$. Candidate target genes (220 for TRB4/*trb4 trb5*; 595 for TRB1/*trb1 trb2 trb3*) are indicated.

(G) Enrichment of *trb4 trb5* ($n = 220$) and *trb1 trb2 trb3* DEGs ($n = 595$) that are direct targets of the respective TRB protein in the nine CSs defined by Sequeira-Mendes et al. (2014); *OR > 1 and $p < 0.01$.

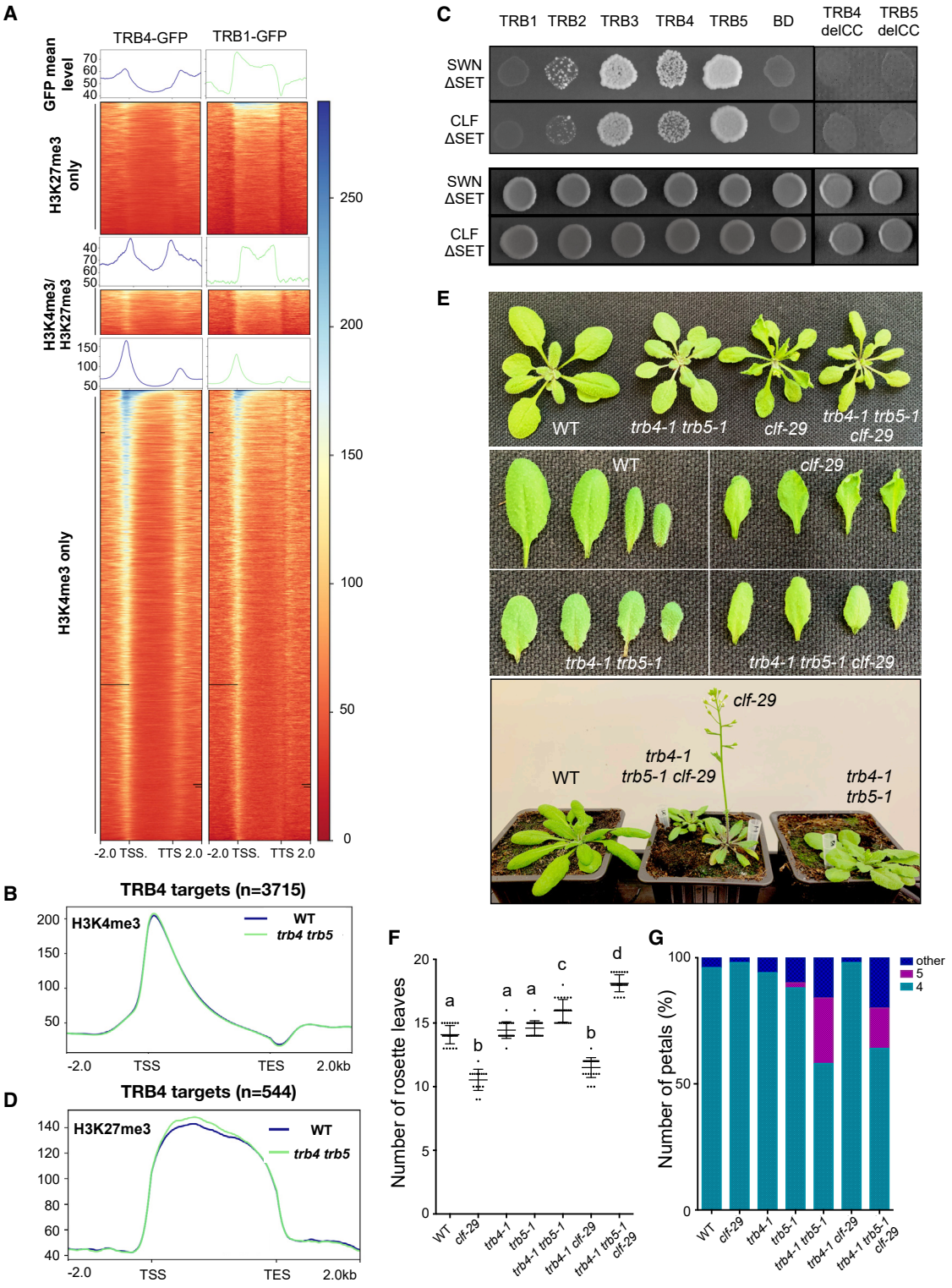

Figure 6. *TRB4* and *TRB5* are required for leaf curling and early flowering in *clf-29 mutant plants*

(A) Metagene plots and heatmaps showing ChIP-seq signals of TRB4-GFP or TRB1-GFP over genes enriched in H3K27me3, H3K4me3, or both histone marks as determined by ChIP-seq analysis.

(B) Metagene plot showing enrichment of H3K4me3 over TRB4-target genes.

(C) Interaction of *Arabidopsis* TRB1–5, TRB4delCC, and TRB5delCC (lacking the coiled-coil domain) proteins (as bait) with CURLY LEAF (CLF) and SWINGER (SWN) proteins (lacking the SET domain) (as prey) probed in the Y2H system. Upper panel: yeast strains growing on synthetic medium lacking

(legend continued on next page)

of genes, both proteins marked the TSSs of genes associated with H3K4me3 (Figure 6A; Supplemental Figure 6A). Given these observations and the demonstrated role of TRB1–3 proteins in H3K4me3 removal (Wang et al., 2023), we tested whether loss of TRB4/5 would affect genome-wide H3K4me3 enrichment. Immunostaining (Supplemental Figure 6B) and H3K4me3 ChIP-seq (Supplemental Figure 6D) revealed that global H3K4 trimethylation patterns were globally unaffected in young *trb4 trb5* plantlets and that only a few genes (n = 120) showed significant changes in this histone mark. Furthermore, plotting H3K4me3 specifically at direct TRB4 targets confirmed that enrichment in this mark was generally maintained in the double mutant (Figure 6B). Therefore, in contrast to the increased level of H3K4me3 reported in the *trb1 trb2 trb3* mutant (Wang et al., 2023) and despite the enrichment of TRB4 at genes marked by H3K4me3, loss of TRB4 and TRB5 did not affect H3K4me3 levels at most TRB4 binding sites, suggesting that modulation of H3K4 methylation or demethylation is not their major mode of action.

Loss of TRB4 and TRB5 rescues leaf curling and early flowering in *clf-29* mutants

TRB2 and TRB3 proteins have previously been shown to interact directly with the PRC2 components CLF and SWN via their coiled-coil domain (Zhou 2018). Because TRB4 and TRB5 differ from clade I TRBs in their coiled-coil domain region (Figure 1D; Supplemental Figure 1B and 1C), we tested whether they could still be engaged in similar interactions. TRB4 and TRB5 interacted with both CLF and SWN in Y2H assays, and this interaction also required the coiled-coil domain (Figure 6C; Supplemental Figure 6F), suggesting that clade II TRBs could indeed recruit PRC2 to chromatin, similar to clade I TRBs or, alternatively, could compete with clade I TRBs for PRC2 interaction.

To investigate whether TRB4 and TRB5 contribute to H3K27me3 enrichment, we profiled the genome-wide distribution of H3K27me3 in 7-day-old WT and mutant plantlets. Immunostaining (Supplemental Figure 6C) and ChIP-seq (Supplemental Figure 6E) indicated that most genes, including TRB4 target genes, retained WT levels of this histone mark in *trb4-1 trb5-1* mutant plants (Figure 6D). Only about 200 genes (2.7%) showed significant H3K27me3 gain or loss. Hence, compared with the *trb1 trb2 trb3* mutant, in which 22% of the H3K27me3-enriched genes showed altered H3K27 methylation (Zhou et al., 2018), the absence of TRB4 and TRB5 affected H3K27me3 at a smaller subset of genes at this developmental stage.

Consistent with the critical function of TRB1–3 in H3K27me3 deposition, loss of TRB1 and TRB3 causes an exacerbation of the *clf-28* single-mutant phenotype (Zhou et al., 2018). To investigate the relationship between PcG function and TRB4 and TRB5, we crossed the double *trb4-1 trb5-1* mutant with *clf-29* (Schönrock et al., 2006). Surprisingly, and in contrast to *trb1* mutants (Zhou et al., 2018), several of the phenotypic features of *clf-29* were rescued by removal of TRB4 and TRB5. The triple-mutant plants did not show downward curled leaves or early flowering; instead, flowering was further delayed compared with that of the *trb4-1 trb5-1* double mutant (Figure 6E and 6F). We confirmed these observations in an independent cross of the *clf-29* mutant with the *trb4-2 trb5-2* double mutant (Supplemental Figure 6G). Our RNA-seq analysis indicated that the phenotypic rescue was not an indirect consequence of misregulation of genes encoding subunits of the PRC2 and PRC1 complexes, as none of the major protein-coding genes of these complexes was misexpressed in the two independent *trb4 trb5* double mutants (Supplemental Table 4). Although the phenotypic defects of *clf-29* were rescued by the loss of TRB4 and TRB5, the *clf-29* mutation did not reciprocally reverse the developmental defects specific to the *trb4 trb5* double mutant, such as the altered leaf color and the supernumerary petal phenotype (Figure 6G). These clade II TRB phenotypes are therefore likely to be caused by PcG-independent processes and tend to be dominant over *clf-29* phenotypes. Thus, TRB4 and TRB5 physically interact with CLF and SWN, two major H3K27 histone methyltransferases, affect H3K27me3 at a small set of genes, and are required for the leaf morphology and flowering defects that characterize the *clf-29* mutant.

TRB4 and TRB5 are required for transcriptional activation of CLF-controlled genes

Flowering time control involves a complex regulatory network that integrates endogenous factors and environmental cues and requires the interplay of chromatin modifications, including the PcG pathway, and TFs at key flowering regulator genes. To gain insight into the complex relationship between PRC2-CLF complexes and clade II TRBs in the control of flowering regulators, we investigated the expression of *SEPALLATA3* (*SEP3*), *FLOWERING LOCUS T* (FT), and SOC1, which are targets of TRB4, and *AGAMOUS* (*AG*), which is responsible for leaf curling (Goodrich et al., 1997) but not a TRB4 target, in the three mutant conditions (*clf-29*, *trb4-1 trb5-1*, and the *trb4-1 trb5-1 clf-29* triple mutant). We extracted RNA from mature leaves of plants before bolting, when these flowering regulators are expressed, and determined relative transcript levels by RT–qPCR. In agreement with tight control by the PcG machinery (Goodrich et al., 1997; Jiang et al., 2008; Lopez-Vernaza et al., 2012), all four genes were upregulated in the *clf-29* mutant, consistent with loss of H3K27me3 (Supplemental Figure 7A). Whereas expression of *SEP3* and *AG* was unchanged in the absence of TRB4 and TRB5, loss of clade II TRBs led to reduced *FT* and *SOC1* transcript levels; however, this decrease was not correlated with H3K27me3 enrichment (Figure 7A; Supplemental

Leu, Trp, and His reveal interactions. Lower panel: growth of zygotes on synthetic medium lacking Leu and Trp, selecting for the presence of the bait and prey vectors for interactions.

(D) Metagene plot showing enrichment of H3K27me3 over TRB4-target genes.

(E) Representative WT, *trb4-1 trb5-1*, *clf-29*, and *trb4-1 trb5-1 clf-29* triple-mutant plants at 3 weeks (top, middle) and 4 weeks (bottom) after sowing. Loss of TRB4 and TRB5 in the *clf-29* mutant background abolishes the curly leaf and early-flowering phenotypes.

(F) Mean number of rosette leaves at bolting in the indicated genotypes.

(G) Mean number of petals observed in flowers from the indicated genotypes.

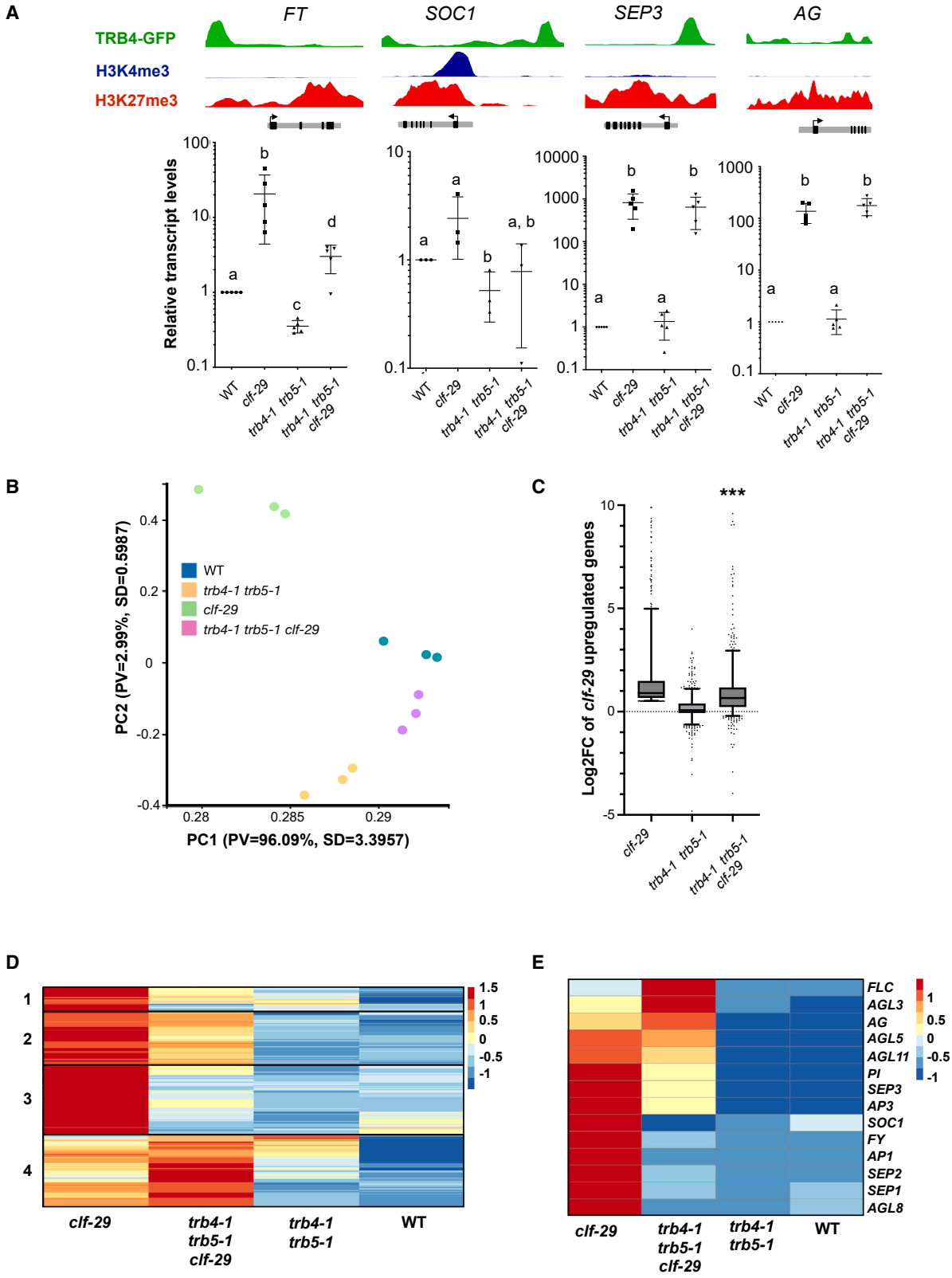

Figure 7. TRB4 and TRB5 function as transcriptional activators of *FT* and *SOC1* flowering regulators

(A) Top: Genome Browser views showing binding of TRB4 and enrichment in H3K4me3 and H3K27me3 at *FLOWERING LOCUS T* (*FT*), *SUPPRESSOR OF OVEREXPRESSION OF CO 1* (*SOC1*), *SEPALLATA3* (*SEP3*), and *AGAMOUS* (*AG*) as determined by ChIP-seq in 7-day-old seedlings. Bottom: relative

(legend continued on next page)

Figure 7A). Compared with *clf-29* single mutants, the *trb4-1 trb5-1 clf-29* triple mutant had reduced *SEP3* (−18%), *SOC1* (−48%), and *FT* (−76%) transcript levels. Together, these results indicate that clade II TRB proteins can function as transcriptional activators of some flowering regulators in both the WT and *clf-29* backgrounds.

To investigate whether TRB4 and TRB5 are required for the transcriptional changes induced by CLF loss in a more global manner, we profiled the transcriptomes of 3-week-old rosette leaves from WT, *clf-29*, *trb4-1 trb5-1*, and *trb4-1 trb5-1 clf-29* plants. Evaluation of transcriptomic patterns by principal-component analysis revealed that loss of TRB4 and TRB5 activity globally suppressed transcriptional changes in *clf-29* (Figure 7B). Likely direct target genes of CLF, which are marked by H3K27me3 in WT plants and are upregulated upon CLF loss (n = 762), tended to show lower expression in the triple-mutant plants (Figure 7C). Indeed, a closer look at the expression changes by *Z*-score clustering showed that, although TRB4 and TRB5 led to a further increase in transcript levels for 23% of these genes, transcript levels for the majority of genes (77%, 585 out of 762) were reduced in the triple mutant compared with the *clf-29* single mutant (Figure 7D).

Of the 1249 upregulated genes in *clf-29*, 14 were MADS-box genes. Within this group, nine genes, including *SOC1,* were significantly downregulated in the *trb4-1 trb5-1 clf-29* triple mutant (Figure 7E). In particular, *SEP3* expression showed a notable two-fold decrease (log2FC [L2FC] = −0.99) in the triple mutant compared with *clf-29*. In addition, *SEP1* and *SEP2*, homologs of *SEP3*, showed a highly significant decrease in expression (L2FC = −2.4 for *SEP1* and L2FC = −4.2 for *SEP2*). These three *SEP* genes are known to play partially redundant roles in controlling *Arabidopsis* development, and their reduced expression likely contributed to the observed reversal of the curly leaf phenotype.

Taken together, our observations point to multifaceted interactions of clade II TRBs with other members of the TRB family and with the PcG machinery that mediate control of development and growth, including flowering time regulation. Our results showed that TRB4 and TRB5 proteins act as novel transcriptional regulators of floral integrators, including *FT* and MADS-box genes, revealing their roles in developmental regulation and fine-tuning of flowering time.

DISCUSSION

TRB4 and TRB5 do not play a major role in telomere protection

The five *Arabidopsis* TRBs, including TRB4 and TRB5, contain two DNA-binding domains: an N-terminal Myb/SANT domain and a central GH1 domain (Kotlinski et al., 2017). In humans, the Myb/SANT domain, which mediates interactions with telomeric double-stranded DNA, can be found in only two proteins, TRF1 and TRF2, which form the core of the ''shelterin'' complex, a complex of six proteins dedicated to telomere protection (Palm and Lange, 2008). In *Arabidopsis thaliana*, in addition to the five TRBs, 12 other proteins harbor the Myb/SANT domain (Schrumpfová et al., 2019), and despite numerous studies, no true shelterin has yet been isolated in plants. For example, absence of TRB1–3 (Zhou et al., 2018; our unpublished data) or of the six TRF-like proteins (Fulcher and Riha, 2016) does not lead to telomere deprotection. We initially identified TRB4 and TRB5 in a pull-down experiment designed to identify telomeric DNA-binding proteins, and their ability to bind telomeric repeats was confirmed by electrophoretic mobility shift assays (Kusová et al., 2023). This study also revealed that TRB4 and TRB5 can interact with the catalytic subunit of telomerase (TERT) as well as several telomerase-interacting proteins (POT1Aa, POT1b, RUVBL1, and RUVBL2A), suggesting that TRB4 and TRB5 are part of the telomerase complex, as has been shown for TRB1–3 proteins (Schrumpfová et al., 2014). However, combined depletion of TRB4 and TRB5 does not affect telomere protection. Therefore, either true shelterin proteins still remain to be identified or deletion of only some members of the TRB family is not sufficient, owing to functional redundancy. In future studies, it will be interesting to investigate whether telomere deprotection contributes to the lethality of *trb1 trb4 trb5* mutants.

Although telomere protection is ensured even in the absence of either clade I or clade II TRBs, plant development and gene expression are affected in the *trb1 trb2 trb3* and *trb4 trb5* mutants, suggesting a role for TRB proteins beyond telomere function. Such a function for telomere proteins is not restricted to plants, as it recalls the role of telomeric proteins in transcriptional silencing of genes located near telomeres in humans and yeast (Gottschling et al., 1990; Robin et al., 2014). For instance, scRAP1, a yeast transcription factor of the MYB superfamily, not only controls telomere function but also activates highly expressed ribosomal protein and glycolytic genes (Azad and Tomar, 2016). ZBTB48, one of the most conserved factors associated with telomeres in human, also acts as a transcriptional activator (Jahn et al., 2017). More recently, mammalian TRF2 was shown to bind to short telomeric sequences in gene promoters, participate in the deposition of active (H3K4me1 and H3K4me3) as well as repressive marks (H3K27me3), and affect the transcription of these genes (Simonet et al., 2011; Mukherjee et al., 2018; Mukherjee et al., 2019). Although TRF2 affects the expression of only a small proportion of genes by an as-yet-unknown mechanism, the control of transcription by telomeric factors appears to be a conserved function among eukaryotes.

transcript levels of *FT*, *SOC1*, *SEP3*, and *AG* in rosette leaves from WT, *trb4-1 trb5-1*, *clf-29*, and *trb4-1 trb5-1 clf-29* triple-mutant plants at 3 weeks of age as determined by RT–qPCR. Different letters indicate significant differences among samples by the Mann–Whitney test ($p < 0.01$).

(B) Principal component analysis of transcriptomes generated from 3-week-old rosette leaves of WT, *trb4-1 trb5-1*, *clf-29*, and *trb4-1 trb5-1 clf-29* triple-mutant plants.

(C) Boxplot presenting log2FC relative to WT for genes upregulated in *clf* mutants and enriched in H3K27me3 (n = 762) in *trb4-1 trb5-1*, *clf-29*, and *trb4-1 trb5-1 clf-29* triple-mutant plants (***$p < 0.0001$, Mann–Whitney test between *clf29* and *trb4-1 trb4-1 clf29* mutants).

(D) *Z*-score hierarchical clustering heatmap of the same genes as in **(C)**.

(E) *Z*-score hierarchical clustering heatmap of the MADS-box genes upregulated in the *clf29* mutant.

TRB origins and evolution

TRB proteins are plant-specific proteins that appeared early in plant evolution, as shown by our phylogenetic analyses and those of others (Kotlinski et al., 2017; Kusová et al., 2023). In an ancestor of spermatophytes, the TRB protein family split into two clades: clade I, which contains *Arabidopsis* TRB1–3, and clade II, which contains *Arabidopsis* TRB4–5. Although all TRB proteins share a common global architecture with three major domains, we have revealed divergences between the two clades and their functional specialization. The TRB clades are mainly distinguished by their C-terminal coiled-coil domains, which mediate the interaction of clade I (Zhou et al., 2018; Kusová et al., 2023) and clade II TRBs (this study) with the catalytic subunits of the PRC2 complex (Zhou et al., 2018; Kusová et al., 2023). They may also enable TRB4 and TRB5 to bind to additional, specific partners that remain to be discovered. Almost all angiosperm genomes, with the sole exception of *Ananas comosus*, encode at least one member of each clade, suggesting a requirement for a balance between the different functions performed by members of the two TRB clades.

TRBs interact with each other and with DNA

Expression analysis does not indicate any tissue-specific expression of the five *TRB* genes during plant development, except for the higher *TRB1* transcript levels observed in the embryo and endosperm. Therefore, the different TRB proteins could be present simultaneously in a given cell. Our results and those of others (Kusová et al., 2023) revealed that all TRB proteins physically interact with each other, both in the yeast system and *in planta*. Although a single telobox motif is sufficient for TRB proteins to bind DNA *in vitro* (Kusová et al., 2023), TRBs may bind simultaneously as multimers or compete with each other for the same sites. Given that TRB hetero- and homodimer formation is likely to occur via the GH1 domain, as demonstrated for TRB1 homodimerization (Schrumpfová et al., 2014), we can postulate that certain genomic sites are simultaneously bound by TRB proteins from both clades. TRB1 or TRB4 could bind DNA via its Myb/SANT domain and interact with another TRB protein via its GH1 domain. Alternatively, several TRB proteins could bind to the same gene via multiple telobox motifs, adjacent telobox and site II motifs, or in a non-sequence-specific manner via the GH1 domain.

Finally, binding to the same sites at different time points or in different tissues, which is not resolved by bulk-tissue ChIP-seq analysis, could also be consistent with the observed co-occurrence of TRB1 and TRB4. Our ChIP-seq experiments showed that TRB proteins from the two clades have both common and specific targets. Therefore, small differences in their respective DNA-binding domains, the chromatin environment, or interactions with specific partners may influence their localization on chromatin.

TRBs have specific and redundant roles

If clade I and clade II TRB proteins coordinately regulate gene expression, we would expect a set of DEGs common to *trb1 trb2 trb3* and *trb4 trb5* mutants, which was the case for a fraction of genes (Figure 2E). However, most of the misregulated genes were specific to an individual mutant, suggesting both common and specific roles for each clade.

Previously, all TRB clade I proteins were suggested to have redundant functions. Indeed, TRB1–3 are highly co-localized throughout the genome (Wang et al., 2023), and the severe developmental defects observed in the triple *trb1 trb2 trb3* mutants can be complemented by any of the TRB clade I proteins. Here, we showed that the *trb2 trb3 trb4 trb5* quadruple mutant is viable but that the *trb1 trb4 trb5* triple mutant is not, demonstrating a specific function of TRB1 that, in the absence of TRB4 and TRB5, cannot be fulfilled by TRB2 or TRB3. A specific role for TRB1 was supported by the fact that TRB1 was present in all the dicots analyzed, whereas TRB2 and TRB3, which appeared after a more recent duplication, were absent in several plant species, such as tomato (Figure 1). Overall, our results indicate that proteins from the two clades may share essential roles. However, further analyses are required to decipher whether the observed lethality of the *trb1 trb4 trb5* triple mutant is related to a defect in gene transcriptional control at a critical embryonic stage or to some other factor, such as telomere deprotection. A scenario is therefore emerging in which proteins from the two different clades work together or play opposing roles in coordinating the expression of target genes. Identifying both the physical and genetic interactors of each TRB may shed light on their specific functions.

Clade II TRB proteins function as transcriptional regulators

Clade I TRB proteins have been shown to recruit histone modifiers (PRC2, JMJ14) to silence a subset of developmental genes by participating in H3K27me3 deposition and H3K4me3 removal (Zhou et al., 2018; Wang et al., 2023) at promoters and gene bodies that contain telobox DNA motifs. Consistent with this function, loss of all three clade I TRB proteins results in developmental growth defects similar to those of severe PRC2 mutants, and loss of one clade I TRB protein alone is sufficient to enhance *clf* mutant phenotypes (Zhou et al., 2018).

Despite their ability to interact with CLF and SWN (Figure 6C) as well as EMF2 and VRN2 (Kusová et al., 2023), double-mutant plants lacking both clade II TRBs do not show a PRC2 mutant-like phenotype but instead display milder developmental phenotypes such as late flowering or supernumerary petal numbers, which have been reported in mutants deficient in H3K27me3 removal (Carles and Fletcher, 2009; Yan et al., 2018) or H3K4me3 deposition (Alvarez-Venegas et al., 2003). Some phenotypes associated with PRC2 deficiency (early flowering, curly leaves) are even restored to normal in triple *trb4 trb5 clf-29* mutant plants. On the basis of these genetic data and our transcriptome analyses highlighting a role of clade II TRBs in counteracting transcriptional repression of PRC2-controlled genes, we expected to observe altered H3K27me3 and/or H3K4me3 homeostasis. However, these marks were affected at only a small subset of genes upon loss of TRB4 and TRB5, and only a few of the genes showed changes in expression. Together, these findings suggest that modulation of the H3K27me3/H3K4me3 balance is not the major mode of action of clade II TRB proteins.

Instead, restoration of the *clf-29* mutant phenotype could result indirectly from altered expression of other factors involved in chromatin regulation or of certain genes targeted by CLF and TRB4, such as *FT* and *SEP*. Reduced expression of *SEP3* in the *clf ft* background was associated with the suppression of early flowering and leaf curling in *clf* mutant leaves without affecting ectopic *AG* expression, previously suggested to be responsible for the leaf-curling phenotype (Lopez-Vernaza et al., 2012).

In our *trb4 trb5* mutant, we observed a mild reduction in *SEP3* expression and a drastic reduction in *SEP1* and *SEP2* expression. The *Arabidopsis* genome encodes four *SEP* genes (*SEP1–4*) that collectively influence floral organ identity in an additive yet predominantly redundant fashion (Pelaz et al., 2000; Ditta et al., 2004). Thus, the reduction in *FT* and *SEP* gene expression due to absence of TRB4 and TRB5 is likely responsible for rescuing the *clf* phenotype.

Our results thus show that clade II TRBs act as novel transcriptional activators of several flowering regulators required for fine-tuning of flowering time.

A potential mode of action for clade II TRB proteins that could be tested in the future is the recruitment of histone acetylation or deacetylation activity that holds a prominent place in the transcriptional control of PRC2 target genes and participates in correct gene expression throughout plant development (Wang et al., 2014). For instance, CBP, a histone acetyltransferase that acetylates H3K27 (H3K27Ac), antagonizes Polycomb silencing (Tie et al., 2014). Specifically, plants deficient in HAC1 and HAC5, two histone acetyltransferases from the MEDIATOR complex, display developmental defects resembling *trb4 trb5* defects: the plants are small, with delayed flowering and reduced fertility (Guo et al., 2021). As demonstrated for clade I TRBs, TRB4 and TRB5 also interact with members of the PEAT complex (Kusová et al., 2023), which is involved in histone deacetylation to silence heterochromatin (Tan et al., 2018). It has also been reported that TRB2 interacts with HDT4 and HDA6, two histone deacetylases that presumably act in H3K27 deacetylation (Lee and Cho, 2016). Together, these observations suggest that TRB proteins may not only influence the deposition/removal of H3K27me3 and H3K4me3 but also participate in the coordination of histone acetylation/deacetylation in a yet-to-be-defined manner.

The GH1 protein family forms a complex network of proteins

The mode of action of TRB proteins in *A. thaliana* is complicated by the presence of several other proteins that harbor a GH1 domain, namely H1 linker histones and GH1-HMGA proteins (Kotlinski et al., 2017). GH1-HMGA proteins that bind the 5′ and 3′ ends of gene bodies similar to a subset of TRB4 targets (Figure 5) have been implicated in the repression of *FLC* by inhibiting gene loop formation, which facilitates *FLC* transcriptional activation (Zhao et al., 2021). Intriguingly, *FLC* is also upregulated in *trb4 trb5* mutants (Supplemental Figure 2L). According to their role in transcriptional regulation, TRB proteins may therefore also participate in the regulation of gene loops by forming homo/heterodimers between proteins linked to nearby motifs (Xuan et al., 2022).

The globular GH1 domain shared by GH1-HMGA1 and H1 proteins can mediate DNA interaction (Bednar et al., 2017) as well as protein–protein interactions (Schrumpfová et al., 2008), potentially leading to a complex network of interaction/competition among TRBs and multiple other GH1-containing proteins. For example, recent work has already pointed to the antagonistic DNA association of TRB1 and H1 proteins (Teano et al., 2023) and the competition between HMGA1 and H1 (Charbonnel et al., 2018).

MATERIALS AND METHODS

Gene and protein sequences

Orthologs of *A. thaliana* TRB proteins were collected from the following plant species that best represent the evolutionary history of the green lineage: *Arabidopsis lyrata*, *Eutrema salsugineum*, *Schrenkiella parvula*, *Brassica rapa*, *Boechera stricta*, *Capsella grandiflora*, *Descurainia sophioides*, *Diptychocarpus strictus*, *Euclidium syriacum*, *Malcolmia maritima*, *Myagrum perfoliatum*, *Rorippa islandica*, *Stanleya pinnata*, *Thlaspi arvense*, *Prunus persica*, *Glycine max*, *Theobroma cacao*, *Vitis vinifera*, *Populus trichocarpa*, *Solanum lycopersicum*, *Oryza sativa*, *Zea mays*, *Sorghum bicolor*, *A. comosus*, *Musa acuminata*, *Amborella trichopoda*, *Nymphaea colorata*, *Pseudotsuga menziesii*, *Picea sitchensis*, *Pinus lambertiana*, *Gnetum momentum*, *Marchantia polymorpha*, *Physcomitrella patens*, *Oestrococcus lucimarinus*, and *Chlamydomonas reinhardtii*. Orthologous sequences were obtained using several sources, including MMseqs (Hauser et al., 2016), NCBI (tblastn and blastp), and Phytozome 13 (Goodstein et al., 2012). Gymnosperm orthologs were identified using the Conifer Genome Integrative Explorer (Sundell et al., 2015).

Protein accession numbers and sequences used in this study are listed in Supplemental Table 1.

Phylogenetic studies

Phylogenetic trees were constructed using protein sequences from Brassicaceae only or from species representing the whole plant lineage; MAFFT 7.407 (Katoh and Standley, 2013) was used for multiple alignment, and IQ-TREE v2.2.0.3 (Minh et al., 2020) was used for tree construction with the LG substitution model and 1000 bootstrap replicates. Trees were refined using the Interactive Tree Of Life (Letunic and Bork, 2016). The Multiple Em for Motif Elicitation (MEME 5.1.1) suite was used for *de novo* motif predictions of TRB protein sequences from Brassicaceae (Bailey, 2021). From a list of orthologous proteins, MEME was parameterized to define 10 motifs, each with a maximum length of 150 amino acids, using the zoops option.

Plant material

The single-mutant lines *trb1-1* (SALK_025147), *trb2-1* (FLAG_242F11), *trb3-1* (SALK_134641), *clf-29* (SALK_021003), and *gh1-hmga1* (SALK_099887C) were provided by the Nottingham *Arabidopsis* Stock Center. The *trb1-1 trb2-1 trb3-1* triple mutant was obtained by crossing. CRISPR-Cas9 technology as described in Fauser et al. (2012) was used to generate the *trb4* and *trb5* single mutants with a single guide RNA (Supplemental Table 3) targeting the first exon of *TRB4* (*At1g17520*) and the second exon of *TRB5* (*At1g72740*; Supplemental Figure 2A). Two single mutants with nucleotide insertions that caused premature stop codons were retained for each gene (Supplemental Figure 2A), and two different double mutants, *trb4-1 trb5-1* and *trb4-2 trb5-2*, were generated by crossing.

For construction of *trb* multiple mutants, *trb4-1 trb5-1* was crossed with *trb1-1*, *trb2-1*, and *trb3-1* single mutants. *trb4-1 trb5-1 trb2-1* and *trb4-1 trb5-1 trb3-1/TRB3* were then crossed to obtain *trb4-1 trb5-1 trb2-1 trb3-1* quadruple mutants.

For plant culture in soil, seeds were stratified for 2 days at 4°C in the dark, and plants were grown under long-day conditions (16-h light, 8-h dark, 23°C). For RNA-seq and ChIP-seq experiments, seeds were sterilized in 70% EtOH/0.01% SDS, and seedlings were grown *in vitro* on 1× MS plates containing 1% sucrose. Transgenic plants were obtained by the floral dip method using *Agrobacterium tumefaciens* strain GV3101, and transgenic progeny were selected using Basta or hygromycin.

Description of plant developmental phenotypes

Root length was measured at 3, 5, and 7 days after germination on three independent replicates of 100 plants each. Seed number per silique was counted on 15 siliques taken from the principal stem of five individual plants. Flowering time was determined by counting the total number of rosette leaves at bolting (30 plants from two independent experiments). The number of petals was counted on 100 flowers from five individual plants. A *t-test* was used to test for significant differences in all parameters except root length, for which a two-way ANOVA was used.

TRF analysis

TRF analysis of telomere length in HinfI-digested genomic DNA was performed as described previously (Charbonnel et al., 2018). TRF scan analyses were carried out using the Web-based Analyser of the Length of Telomeres (WALTER) toolset (Lyčka et al., 2021).

Constructs and cloning

All cloning procedures relied on Gateway technology. For *in planta* complementation of the *trb4-1 trb5-1* and *trb4-2 trb5-2* double mutants, genomic constructs were obtained by PCR amplification from genomic DNA. Constructs containing either the respective endogenous promoter or the *HMGA2* (*At1g48620*) promoter (used for IF and ChIP-seq) were generated and cloned into pDONR vectors.

For Y2H and BiFC constructs, the cDNA of *TRB5* was obtained by RT–PCR. The cDNA of *TRB4* was synthesized (Integrated DNA Technologies, https://eu.idtdna.com/). After initial cloning into pDONR, constructs were recombined into the appropriate expression vectors for Y2H assays (bait vector pDEST-GBKT7 or prey vector pDEST-GADT7), for *in planta* expression (pB7FWG), or for BiFC (pBiFCt-2in1-NN). The list of all plasmids and oligonucleotides used in this study can be found in Supplemental Table 3.

Y2H assay

Yeast cultures were grown at 30°C on YPD or on selective SD medium. Bait (pDEST-GBKT7) or prey (pDEST-GADT7) vectors were transformed into *Saccharomyces cerevisiae* strains AH109 Gold and Y187 (Clontech, MATCHMAKER GAL4 Two-Hybrid System), respectively, using a classical heat-shock protocol (Gietz and Woods, 2002) and grown on selective medium lacking Trp or Leu. The two yeast strains were mated on YPD, and diploids were selected on SD-Leu-Trp. Protein–protein interactions were detected by growth on low-stringency selective medium lacking Leu, Trp, and His. Empty pDEST-GBKT7 or pDEST-GADT7 vectors were used as negative controls.

BiFC

BiFC vectors were transformed into *A. tumefaciens* strain GV3101, and *Agrobacterium* was infiltrated into young *N. benthamiana* leaves as described previously (Grefen and Blatt, 2012), together with the p19 suppressor of gene silencing to enhance expression (Norkunas et al., 2018).

Slide preparation and immunofluorescence staining

For immunostaining of H3K4me3, H3K27me3, and γ-H2A.X and detection of TRB-GFP fusion proteins, nuclei from 7-day-old seedlings were isolated as described in Pavlova et al. (2010). Slides were incubated overnight at 4°C with 50 μl of primary antibody in fresh blocking buffer (3% BSA, 0.05% Tween 20 in 1× PBS), washed 3 times for 5 min each in 1× PBS solution, and then incubated for 2–3 h at room temperature in 50 μl of blocking buffer containing secondary antibodies. Finally, slides were washed 3 times for 5 min each in 1× PBS and mounted in Vectashield mounting medium with 1.5 μg/ml DAPI (Vector Laboratories). Antibodies and dilutions used in this study are described in Supplemental Table 3. For γ-H2A.X immunostaining, root tips from 7-day-old plantlets were treated as described in Amiard et al. (2011), and the foci were counted for 100 nuclei from five individual plants of each genotype. For quantification of anaphase bridges, whole inflorescences were treated as described in Amiard et al. (2011). At least 100 mitoses were counted from five individual plants.

Image acquisition and analysis

For the BiFC analysis, fluorescence images of transiently transfected *N. benthamiana* leaves were obtained using an inverted confocal laser-scanning microscope (LSM 800; Carl Zeiss). The 488-nm line of a 40-mW Ar/Kr laser and the 544-nm line of a 1-mW He/Ne laser were used to excite GFP/YFP and RFP (transfection control), respectively. Images were acquired with a 20× or 40× objective. Images of *Arabidopsis* roots expressing TRB4- or TRB5-GFP or immunostained isolated nuclei were acquired with a Zeiss epifluorescence microscope equipped with an Apotome device using a 20× objective or a 63× oil-immersion objective, respectively.

RNA extraction, RT–qPCR, and sequencing

Seven-day-old *in vitro*-grown plantlets or adult leaves of soil-grown 3- to 4-week-old plants were ground in 2-ml tubes using a Tissue Lyser (Qiagen) twice for 30 s at 30 Hz before RNA extraction using the RNeasy Plant Mini kit (Qiagen). For RT–qPCR, RNA was primed with oligo(dT)15 using M-MLV reverse transcriptase (Promega, https://france.promega.com). Relative transcript levels were determined with the LightCycler 480 SYBR Green I Master kit (Roche, https://lifescience.roche.com) on the Roche LightCycler 480 after normalization to *MON1* (*At2g28390*) transcript levels using the comparative threshold cycle method. Primers used for RT–qPCR can be found in Supplemental Table 3.

For RNA-seq analysis, mRNA was sequenced using the DNBseq platform at the Beijing Genomics Institute (BGI Group) to obtain approximately 20 million 150-bp paired-end, strand-specific reads. Differential expression was determined using an in-house pipeline (https://github.com/vindarbot/RNA_Seq_Pipeline). In brief, reads were trimmed using BBDuk (Bushnell, 2014) to remove adapters and low-quality reads. Clean reads were then aligned to the TAIR10 genome using STAR (v2.7.1). Read counts per gene were generated using featureCounts (v1.6.3), and differential expression analysis was performed with DESeq2 (Love et al., 2014) using the threshold log2FC > 0.5 and adjusted p <0.01. GO-term enrichment analysis of differentially regulated genes was performed with ClusterProfiler (Wu et al., 2021) using all expressed genes in the dataset as the background list.

ChIP–qPCR and ChIP-seq

ChIP-seq analysis was carried out essentially as described in Teano et al. (2023). In brief, about 1 g of 7-day-old *in vitro*-grown plantlets were fixed in 1% formaldehyde under vacuum twice for 7 min and then quenched in 0.125 M glycine. Nuclei were isolated and lysed, and chromatin was sonicated using the Diagenode Bioruptor (set to high intensity, three times seven cycles, 30 s on/30 s off) or the S220 Focused-ultrasonicator (Covaris) for 20 min at peak power 110 W, duty factor 5%, 200 cycles per burst for TRB4-GFP and for 5 min at peak power 175 W, duty factor 20%, 200 cycles per burst for histone modifications to obtain mono-nucleosomal fragments. The following antibodies were used for immunoprecipitation: anti-GFP, Invitrogen, #A-111222; anti-H3K27me3, Diagenode, #C15410069, Batch A1818P; anti-H3K4me3, Millipore #04-745. Immunoprecipitated DNA was recovered by phenol–chloroform extraction or Zymo ChIP DNA purification columns and quantified using a Qubit instrument. Libraries were prepared using the Illumina TruSeq ChIP kit, and sequencing was carried out on the BGI platform (DNBSEQ-G400, 1 × 50 bp). Each ChIP-seq

was performed in two biological replicates. Oligonucleotides used for ChIP–qPCR are listed in Supplemental Table 3. Three biological replicates were performed.

Bioinformatics for ChIP-seq analysis

For the TRB4-GFP ChIP-seq, raw reads were pre-processed with TrimGalore to remove Illumina sequencing adapters. Trimmed reads were mapped against the TAIR10 *A. thaliana* genome with Bowtie 2 with the "–very-sensitive" setting. Peaks were called using MACS2 (Zhang et al., 2008) with the command "macs2 callpeak -f BAM -g 1e8 --nomodel –broad –qvalue 0.01 –extsize 100." Only peaks found in both biological replicates were retained for further analyses (bedtools v2.29.2 intersect). Genes and TEs were annotated using HOMER (annotatePeaks.pl). Metagene plots were generated with deepTools using the computeMatrix and plotProfile commands. TRB4-GFP and TRB1-GFP clusters were identified using deepTools plotHeatmap with the "–kmeans" setting. Motif enrichment under TRB4-GFP peaks was performed using STREME version 5.5.0 (Bailey, 2021) with the following options: "–verbosity 1 –oc –dna –totallength 4000000 –time 14 400 –minw 8 –maxw 15 –nmotifs 10 –align center."

For H3K27me3 and H3K4me3 enrichment analysis, raw reads were aligned with Bowtie 2. Peaks of H3K27me3 read density were called using MACS2 (Zhang et al., 2008) with the command "macs2 callpeak -f BAM –nolambda -q 0.01 -g –broad." Only peaks found in both biological replicates and overlapping by at least 10% were retained for further analyses. We scored the number of H3K27me3 or H3K4me3 reads overlapping with marked genes using bedtools v2.29.2 multicov and analyzed them with the DESeq2 package (Love et al., 2014) in the R statistical environment v4.1.2 to identify the genes enriched or depleted in H3K27me3 or H4K4me3 mutant plants ($p < 0.01$).

DATA AND CODE AVAILABILITY

The genome-wide sequencing data generated in this study have been deposited at the NCBI GEO repository under accession numbers GSE236267 (RNA-seq, *trb4 trb5*, *trb1 trb2 trb3*, 7-day-old seedlings), GSE253005 (RNA-seq, WT, *clf-29*, *trb4-1 trb5-1*, *trb4-1 trb5-1 clf-29*, 3-week-old leaves), GSE237158 (ChIP-seq TRB4-GFP), and GSE237185 (ChIP-seq H3K27me3 and H3K4me3 in WT and *trb4-1 trb5-1*). These series are grouped in the SuperSeries GSE253016. All other data supporting the conclusions of the study will be available from the corresponding author upon request.

SUPPLEMENTAL INFORMATION

Supplemental information is available at *Plant Communications Online*.

FUNDING

We acknowledge funding from ANR grants 4D-HEAT ANR-21-CE20-0036 and EpiLinks ANR-22-CE20-0001, funding from the CAP20-25 Emergence 2019 project, project financing and networking support from the GDR Epiplant, as well as networking support from the COST-Action INDEPTH.

AUTHOR CONTRIBUTIONS

S.A. and A.V.P. designed the research, interpreted the data, and wrote the manuscript. S.A. performed most of the experiments with help from L.F. (BiFC, cloning, phenotyping, RT–qPCR, and ChIP–qPCR), S.L.G. and E.V. (Y2H, BiFC), L.L. (cloning, phenotyping), and L.W. and A.V.P. (ChIP-seq). F.B. performed IP–MS and interpreted the data. S.A., C.B., F.B., L.S., and C.T. performed bioinformatic data analyses. S.A., F.B., and A.V.P. reviewed the manuscript.

ACKNOWLEDGMENTS

We thank Yoan Renaud for help and advice with the bioinformatics analysis and Aurore Pardon and Vincent Darbot for technical help. We thank Claire Jourdain and Daniel Schubert for sharing the CLF and SWN constructs for Y2H and Charles White and Maria Gallego for support and advice during the initial stages of this project. We also thank the CLIC, the Anipath histopathologie, and the plant platforms of the iGRED. No conflict of interest is declared.

Received: August 6, 2023
Revised: February 7, 2024
Accepted: March 29, 2024
Published: April 1, 2024

REFERENCES

Alvarez-Venegas, R., Pien, S., Sadder, M., Witmer, X., Grossniklaus, U., and Avramova, Z. (2003). ATX-1, an Arabidopsis Homolog of Trithorax, Activates Flower Homeotic Genes. Curr. Biol. **13**:627–637.

Amiard, S., Depeiges, A., Allain, E., White, C.I., and Gallego, M.E. (2011). Arabidopsis ATM and ATR kinases prevent propagation of genome damage caused by telomere dysfunction. Plant Cell **23**:4254–4265.

Ariel, F., Jegu, T., Latrasse, D., Romero-Barrios, N., Christ, A., Benhamed, M., and Crespi, M. (2014). Noncoding Transcription by Alternative RNA Polymerases Dynamically Regulates an Auxin-Driven Chromatin Loop. Mol. Cell **55**:383–396.

Azad, G.K., and Tomar, R.S. (2016). The multifunctional transcription factor Rap1 a regulator of yeast physiology. Front. Biosci. **21**:918–930.

Baile, F., Gómez-Zambrano, Á., and Calonje, M. (2022). Roles of Polycomb complexes in regulating gene expression and chromatin structure in plants. Plant Commun. **3**, 100267.

Bailey, T.L. (2021). STREME: accurate and versatile sequence motif discovery. Bioinformatics **37**:2834–2840.

Bednar, J., Garcia-Saez, I., Boopathi, R., Cutter, A.R., Papai, G., Reymer, A., Syed, S.H., Lone, I.N., Tonchev, O., Crucifix, C., et al. (2017). Structure and Dynamics of a 197∼bp Nucleosome in Complex with Linker Histone H1. Mol. Cell **66**:384–397.e8.

Berger, N., Dubreucq, B., Roudier, F., Dubos, C., and Lepiniec, L. (2011). Transcriptional Regulation of Arabidopsis LEAFY COTYLEDON2 Involves RLE , a cis -Element That Regulates Trimethylation of Histone H3 at Lysine-27. Plant Cell **23**:4065–4078.

Bouyer, D., Roudier, F., Heese, M., Andersen, E.D., Gey, D., Nowack, M.K., Goodrich, J., Renou, J.-P., Grini, P.E., Colot, V., and Schnittger, A. (2011). Polycomb Repressive Complex 2 Controls the Embryo-to-Seedling Phase Transition. PLoS Genet. **7**, e1002014.

Bushnell. (2014). BBMap: A Fast, Accurate, Splice-Aware Aligner (Lawrence Berkeley National Laboratory). *LBNL Report #: LBNL-7065E. Retrieved from*. https://escholarship.org/uc/item/1h3515gnAdvance.

Carles, C.C., and Fletcher, J.C. (2009). The SAND domain protein ULTRAPETALA1 acts as a trithorax group factor to regulate cell fate in plants. Gene Dev. **23**:2723–2728.

Carles, C.C., Choffnes-Inada, D., Reville, K., Lertpiriyapong, K., and Fletcher, J.C. (2005). ULTRAPETALA1 encodes a SAND domain putative transcriptional regulator that controls shoot and floral meristem activity in Arabidopsis. Development **132**:897–911.

Chanvivattana, Y., Bishopp, A., Schubert, D., Stock, C., Moon, Y.-H., Sung, Z.R., and Goodrich, J. (2004). Interaction of Polycomb-group proteins controlling flowering in Arabidopsis. Development **131**:5263–5276.

Charbonnel, C., Rymarenko, O., Da Ines, O., Benyahya, F., White, C.I., Butter, F., and Amiard, S. (2018). The Linker Histone GH1-HMGA1 Is

Involved in Telomere Stability and DNA Damage Repair. Plant Physiol. **177**:311–327.

Davidovich, C., and Cech, T.R. (2015). The recruitment of chromatin modifiers by long noncoding RNAs: lessons from PRC2. RNA **21**:2007–2022.

Deng, W., Buzas, D.M., Ying, H., Robertson, M., Taylor, J., Peacock, W.J., Dennis, E.S., and Helliwell, C. (2013). Arabidopsis Polycomb Repressive Complex 2 binding sites contain putative GAGA factor binding motifs within coding regions of genes. BMC Genom. **14**:593.

Ditta, G., Pinyopich, A., Robles, P., Pelaz, S., and Yanofsky, M.F. (2004). The SEP4 Gene of Arabidopsis thaliana Functions in Floral Organ and Meristem Identity. Curr. Biol. **14**:1935–1940. https://doi.org/10.1016/j.cub.2004.10.028.

Fauser, F., Roth, N., Pacher, M., Ilg, G., Sánchez-Fernández, R., Biesgen, C., and Puchta, H. (2012). In planta gene targeting. Proc. Natl. Acad. Sci. USA **109**:7535–7540.

Fitzgerald, M.S., Riha, K., Gao, F., Ren, S., McKnight, T.D., and Shippen, D.E. (1999). Disruption of the telomerase catalytic subunit gene from Arabidopsis inactivates telomerase and leads to a slow loss of telomeric DNA. Proc. Natl. Acad. Sci. USA **96**:14813–14818.

Fulcher, N., and Riha, K. (2015). Using Centromere Mediated Genome Elimination to Elucidate the Functional Redundancy of Candidate Telomere Binding Proteins in Arabidopsis thaliana. Front. Genet. **6**:349–1299.

Gaspin, C., Rami, J.-F., and Lescure, B. (2010). Distribution of short interstitial telomere motifs in two plant genomes: putative origin and function. BMC Plant Biol. **10**:283.

Gietz, R.D., and Woods, R.A. (2002). Transformation of yeast by lithium acetate/single-stranded carrier DNA/polyethylene glycol method. Methods Enzymol. **350**:87–96.

Goodrich, J., Puangsomlee, P., Martin, M., Long, D., Meyerowitz, E.M., and Coupland, G. (1997). A Polycomb-group gene regulates homeotic gene expression in Arabidopsis. Nature **386**:44–51.

Goodstein, D.M., Shu, S., Howson, R., Neupane, R., Hayes, R.D., Fazo, J., Mitros, T., Dirks, W., Hellsten, U., Putnam, N., and Rokhsar, D.S. (2012). Phytozome: a comparative platform for green plant genomics. Nucleic Acids Res. **40**:D1178–D1186.

Gottschling, D.E., Aparicio, O.M., Billington, B.L., and Zakian, V.A. (1990). Position effect at S. cerevisiae telomeres: Reversible repression of Pol II transcription. Cell **63**:751–762.

Grefen, C., and Blatt, M.R. (2012). A 2in1 cloning system enables ratiometric bimolecular fluorescence complementation (rBiFC). Biotechniques **53**:311–314.

Guo, J., Wei, L., Chen, S.S., Cai, X.W., Su, Y.N., Li, L., Chen, S., and He, X.J. (2021). The CBP/p300 histone acetyltransferases function as plant-specific MEDIATOR subunits in Arabidopsis. J. Integr. Plant Biol. **63**:755–771.

Hauser, M., Steinegger, M., and Söding, J. (2016). MMseqs software suite for fast and deep clustering and searching of large protein sequence sets. Bioinformatics **32**:1323–1330.

Horard, B., Tatout, C., Poux, S., and Pirrotta, V. (2000). Structure of a Polycomb Response Element and In Vitro Binding of Polycomb Group Complexes Containing GAGA Factor. Mol. Cell Biol. **20**:3187–3197.

Jahn, A., Rane, G., Paszkowski-Rogacz, M., Sayols, S., Bluhm, A., Han, C.T., Drašković, I., Londoño-Vallejo, J.A., Kumar, A.P., Buchholz, F., et al. (2017). ZBTB48 is both a vertebrate telomere-binding protein and a transcriptional activator. EMBO Rep. **18**:929–946, published 2017. https://doi.org/10.15252/embr.201744095.

Jiang, D., Wang, Y., Wang, Y., and He, Y. (2008). Repression of FLOWERING LOCUS C and FLOWERING LOCUS T by the Arabidopsis Polycomb Repressive Complex 2 Components. PLoS One **3**, e3404.

Jumper, J., Evans, R., Pritzel, A., Green, T., Figurnov, M., Ronneberger, O., Tunyasuvunakool, K., Bates, R., Žídek, A., Potapenko, A., et al. (2021). Highly accurate protein structure prediction with AlphaFold. Nature **596**:583–589.

Katoh, K., and Standley, D.M. (2013). MAFFT Multiple Sequence Alignment Software Version 7: Improvements in Performance and Usability. Mol. Biol. Evol. **30**:772–780.

Kotliński, M., Knizewski, L., Muszewska, A., Rutowicz, K., Lirski, M., Schmidt, A., Baroux, C., Ginalski, K., and Jerzmanowski, A. (2017). Phylogeny-Based Systematization of Arabidopsis Proteins with Histone H1 Globular Domain. Plant Physiol. **174**:27–34.

Kusová, A., Steinbachová, L., Přerovská, T., Drábková, L.Z., Paleček, J., Khan, A., Rigóová, G., Gadiou, Z., Jourdain, C., Stricker, T., et al. (2023). Completing the TRB family: newly characterized members show ancient evolutionary origins and distinct localization, yet similar interactions. Plant Mol. Biol. **112**:61–83, Advance Access published 2023. https://doi.org/10.1007/s11103-023-01348-2.

Lee, W.K., and Cho, M.H. (2016). Telomere-binding protein regulates the chromosome ends through the interaction with histone deacetylases in Arabidopsis thaliana. Nucleic Acids Res. **44**:4610–4624.

Letunic, I., and Bork, P. (2016). Interactive tree of life (iTOL) v3: an online tool for the display and annotation of phylogenetic and other trees. Nucleic Acids Res. **44**:W242–W245.

Lewis, E.B. (1978). A gene complex controlling segmentation in Drosophila. Nature **276**:565–570.

Lodha, M., Marco, C.F., and Timmermans, M.C.P. (2013). The ASYMMETRIC LEAVES complex maintains repression of KNOX homeobox genes via direct recruitment of Polycomb-repressive complex2. Gene Dev. **27**:596–601.

Lopez-Vernaza, M., Yang, S., Müller, R., Thorpe, F., de Leau, E., and Goodrich, J. (2012). Antagonistic roles of SEPALLATA3, FT and FLC genes as targets of the polycomb group gene CURLY LEAF. PLoS One **7**, e30715.

Love, M.I., Huber, W., and Anders, S. (2014). Moderated estimation of fold change and dispersion for RNA-seq data with DESeq2. Genome Biol. **15**:550.

Lyčka, M., Peska, V., Demko, M., Spyroglou, I., Kilar, A., Fajkus, J., and Fojtová, M. (2021). WALTER: an easy way to online evaluate telomere lengths from terminal restriction fragment analysis. BMC Bioinf. **22**:145.

Margueron, R., and Reinberg, D. (2011). The Polycomb complex PRC2 and its mark in life. Nature **469**:343–349.

Margueron, R., Justin, N., Ohno, K., Sharpe, M.L., Son, J., Drury, W.J., 3rd, Voigt, P., Martin, S.R., Taylor, W.R., De Marco, V., et al. (2009). Role of the polycomb protein EED in the propagation of repressive histone marks. Nature **461**:762–767.

Michaels, S.D., and Amasino, R.M. (1999). FLOWERING LOCUS C Encodes a Novel MADS Domain Protein That Acts as a Repressor of Flowering. Plant Cell **11**:949–956.

Minh, B.Q., Schmidt, H.A., Chernomor, O., Schrempf, D., Woodhams, M.D., von Haeseler, A., and Lanfear, R. (2020). IQ-TREE 2: New models and efficient methods for phylogenetic inference in the genomic era. Mol. Biol. Evol. **37**:1530–1534.

Mozgová, I., Schrumpfová, P.P., Hofr, C., and Fajkus, J. (2008). Functional characterization of domains in AtTRB1, a putative telomere-binding protein in Arabidopsis thaliana. Phytochemistry **69**:1814–1819.

Mukherjee, A.K., Sharma, S., Sengupta, S., Saha, D., Kumar, P., Hussain, T., Srivastava, V., Roy, S.D., Shay, J.W., and Chowdhury, S. (2018). Telomere length-dependent transcription and epigenetic modifications in promoters remote from telomere ends. PLoS Genet. **14**, e1007782.

Mukherjee, A.K., Sharma, S., Bagri, S., Kutum, R., Kumar, P., Hussain, A., Singh, P., Saha, D., Kar, A., Dash, D., and Chowdhury, S. (2019). Telomere repeat–binding factor 2 binds extensively to extra-telomeric G-quadruplexes and regulates the epigenetic status of several gene promoters. J. Biol. Chem. **294**:17709–17722.

Norkunas, K., Harding, R., Dale, J., and Dugdale, B. (2018). Improving agroinfiltration-based transient gene expression in Nicotiana benthamiana. Plant Methods **14**:71.

Palm, W., and de Lange, T. (2008). How Shelterin Protects Mammalian Telomeres. Annu. Rev. Genet. **42**:301–334.

Pavlova, P., Tessadori, F., de Jong, H.J., and Fransz, P. (2010). Plant Developmental Biology, Methods and Protocols. Methods Mol. Biol. **655**:413–432.

Pelaz, S., Ditta, G.S., Baumann, E., Wisman, E., and Yanofsky, M.F.B. (2000). and C floral organ identity functions require SEPALLATA MADS-box genes. Nature **405**:200–203. https://doi.org/10.1038/35012103.

Robin, J.D., Ludlow, A.T., Batten, K., Magdinier, F., Stadler, G., Wagner, K.R., Shay, J.W., and Wright, W.E. (2014). Telomere position effect: regulation of gene expression with progressive telomere shortening over long distances. Genes Dev. **28**:2464–2476.

Samach, A., Onouchi, H., Gold, S.E., Ditta, G.S., Schwarz-Sommer, Z., Yanofsky, M.F., and Coupland, G. (2000). Distinct Roles of CONSTANS Target Genes in Reproductive Development of Arabidopsis. Science **288**:1613–1616.

Sauvageau, M., and Sauvageau, G. (2008). Polycomb Group Genes: Keeping Stem Cell Activity in Balance. PLoS Biol. **6**:e113.

Schönrock, N., Bouveret, R., Leroy, O., Borghi, L., Köhler, C., Gruissem, W., and Hennig, L. (2006). Polycomb-group proteins repressthe floral activator AGL19 in the FLC-independent vernalization pathway. Gene Dev. **20**:1667–1678.

Schrumpfova, P., Kuchař, M., Mikov, G., Skřšovsk, L., Kubičrov, T., and Fajkus, J. (2004). Characterization of two Arabidopsis thaliana myb-like proteins showing affinity to telomeric DNA sequence. Genome **47**:316–324.

Schrumpfová, P.P., Kuchař, M., Paleček, J., and Fajkus, J. (2008). Mapping of interaction domains of putative telomere-binding proteins AtTRB1 and AtPOT1b from Arabidopsis thaliana. FEBS Lett. **582**:1400–1406.

Schrumpfová, P.P., Vychodilová, I., Dvořáčková, M., Majerská, J., Dokládal, L., Schořová, S., and Fajkus, J. (2014). Telomere repeat binding proteins are functional components of Arabidopsis telomeres and interact with telomerase. Plant J. **77**:770–781.

Schrumpfová, P.P., Vychodilová, I., Hapala, J., Schořová, Š., Dvořáček, V., and Fajkus, J. (2016). Telomere binding protein TRB1 is associated with promoters of translation machinery genes in vivo. Plant Mol. Biol. **90**:189–206.

Schrumpfová, P.P., Fojtová, M., and Fajkus, J. (2019). Telomeres in Plants and Humans: Not So Different, Not So Similar. Cells **8**:58.

Schuettengruber, B., Bourbon, H.-M., Di Croce, L., and Cavalli, G. (2017). Genome Regulation by Polycomb and Trithorax: 70 Years and Counting. Cell **171**:34–57.

Sequeira-Mendes, J., Aragüez, I., Peiró, R., Mendez-Giraldez, R., Zhang, X., Jacobsen, S.E., Bastolla, U., and Gutierrez, C. (2014). The Functional Topography of the ArabidopsisGenome Is Organized in a Reduced Number of Linear Motifs of Chromatin States. Plant Cell **26**:2351–2366.

Shu, J., Chen, C., Li, C., and Cui, Y. (2020). The complexity of PRC2 catalysts CLF and SWN in plants. Biochem. Soc. Trans. **48**:2779–2789.

Simmons, A.R., and Bergmann, D.C. (2016). Transcriptional control of cell fate in the stomatal lineage. Curr. Opin. Plant Biol. **29**:1–8.

Simonet, T., Zaragosi, L.-E., Philippe, C., Lebrigand, K., Schouteden, C., Augereau, A., Bauwens, S., Ye, J., Santagostino, M., Giulotto, E., et al. (2011). The human TTAGGG repeat factors 1 and 2 bind to a subset of interstitial telomeric sequences and satellite repeats. Cell Res. **21**:1028–1038.

Simonini, S., Bemer, M., Bencivenga, S., Gagliardini, V., Pires, N.D., Desvoyes, B., van der Graaff, E., Gutierrez, C., and Grossniklaus, U. (2021). The Polycomb group protein MEDEA controls cell proliferation and embryonic patterning in Arabidopsis. Dev. Cell **56**:1945–1960.e7, published 2021. https://doi.org/10.1016/j.devcel.2021.06.004.

Sundell, D., Mannapperuma, C., Netotea, S., Delhomme, N., Lin, Y.C., Sjödin, A., Van de Peer, Y., Jansson, S., Hvidsten, T.R., and Street, N.R. (2015). The Plant Genome Integrative Explorer Resource: PlantGenIE.org. New Phytol. **208**:1149–1156.

Tan, L.M., Zhang, C.J., Hou, X.M., Shao, C.R., Lu, Y.J., Zhou, J.X., Li, Y.Q., Li, L., Chen, S., and He, X.J. (2018). The PEAT protein complexes are required for histone deacetylation and heterochromatin silencing. EMBO J. **37**:e98770.

Teano, G., Concia, L., Wolff, L., Carron, L., Biocanin, I., Adamusová, K., Fojtová, M., Bourge, M., Kramdi, A., Colot, V., et al. (2023). Histone H1 protects telomeric repeats from H3K27me3 invasion in Arabidopsis. Cell Rep. **42**, 112894.

Tie, F., Banerjee, R., Saiakhova, A.R., Howard, B., Monteith, K.E., Scacheri, P.C., Cosgrove, M.S., and Harte, P.J. (2014). Trithorax monomethylates histone H3K4 and interacts directly with CBP to promote H3K27 acetylation and antagonize Polycomb silencing. Development **141**:1129–1139.

Vijayanathan, M., Trejo-Arellano, M.G., and Mozgová, I. (2022). Polycomb Repressive Complex 2 in Eukaryotes—An Evolutionary Perspective. Epigenomes **6**:3.

Wang, Z., Cao, H., Chen, F., and Liu, Y. (2014). The roles of histone acetylation in seed performance and plant development. Plant Physiol. Biochem. (Issy les Moulineaux, Fr.) **84**:125–133.

Wang, H., Liu, C., Cheng, J., Liu, J., Zhang, L., He, C., Shen, W.-H., Jin, H., Xu, L., and Zhang, Y. (2016). Arabidopsis Flower and Embryo Developmental Genes are Repressed in Seedlings by Different Combinations of Polycomb Group Proteins in Association with Distinct Sets of Cis-regulatory Elements. PLoS Genet. **12**, e1005771.

Wang, M., Zhong, Z., Gallego-Bartolomé, J., Feng, S., Shih, Y.-H., Liu, M., Zhou, J., Richey, J.C., Ng, C., Jami-Alahmadi, Y., et al. (2023). Arabidopsis TRB proteins function in H3K4me3 demethylation by recruiting JMJ14. Nat. Commun. **14**:1736.

Wu, T., Hu, E., Xu, S., Chen, M., Guo, P., Dai, Z., Feng, T., Zhou, L., Tang, W., Zhan, L., et al. (2021). clusterProfiler 4.0: A universal enrichment tool for interpreting omics data. Innovation **2**, 100141.

Xiao, J., Jin, R., Yu, X., Shen, M., Wagner, J.D., Pai, A., Song, C., Zhuang, M., Klasfeld, S., He, C., et al. (2017). Cis and trans determinants of epigenetic silencing by Polycomb repressive complex 2 in Arabidopsis. Nat. Genet. **49**:1546–1552.

Xuan H., Liu L., Zhao J., Shi N., Li Y., Zhou Y., Pi L., Li S., Xu G., Yang H.. Phase-separated TRB-PRC2 aggregates contribute to Polycomb silencing in plants. Preprint at bioRxiv 2022.03.27.485997

Yan, W., Chen, D., Smaczniak, C., Engelhorn, J., Liu, H., Yang, W., Graf, A., Carles, C.C., Zhou, D.-X., and Kaufmann, K. (2018). Dynamic and spatial restriction of Polycomb activity by plant histone demethylases. Nat. Plants **4**:681–689.

Yuan, L., Song, X., Zhang, L., Yu, Y., Liang, Z., Lei, Y., Ruan, J., Tan, B., Liu, J., and Li, C. (2021). The transcriptional repressors VAL1 and VAL2 recruit PRC2 for genome-wide Polycomb silencing in Arabidopsis. Nucleic Acids Res. **49**:98–113.

Zhang, X., Clarenz, O., Cokus, S., Bernatavichute, Y.V., Pellegrini, M., Goodrich, J., and Jacobsen, S.E. (2007). Whole-Genome Analysis of Histone H3 Lysine 27 Trimethylation in Arabidopsis. PLoS Biol. **5**, e129.

Zhang, Y., Liu, T., Meyer, C.A., Eeckhoute, J., Johnson, D.S., Bernstein, B.E., Nusbaum, C., Myers, R.M., Brown, M., Li, W., and Liu, X.S. (2008). Model-based Analysis of ChIP-Seq (MACS). Genome Biol. **9**:R137.

Zhao, B., Xi, Y., Kim, J., and Sung, S. (2021). Chromatin architectural proteins regulate flowering time by precluding gene looping. Sci. Adv. **7**, eabg3097.

Zhou, Y., Hartwig, B., James, G.V., Schneeberger, K., and Turck, F. (2016). Complementary Activities of TELOMERE REPEAT BINDING Proteins and Polycomb Group Complexes in Transcriptional Regulation of Target Genes. Plant Cell **28**:87–101.

Zhou, Y., Wang, Y., Krause, K., Yang, T., Dongus, J.A., Zhang, Y., and Turck, F. (2018). Telobox motifs recruit CLF/SWN–PRC2 for H3K27me3 deposition via TRB factors in Arabidopsis. Nat. Genet. **50**:638–644.

Plant Communications, Volume *5*

Supplemental information

The TELOMERE REPEAT BINDING proteins TRB4 and TRB5 function as transcriptional activators of PRC2-controlled genes to regulate plant development

Simon Amiard, Léa Feit, Emmanuel Vanrobays, Lauriane Simon, Samuel Le Goff, Loriane Loizeau, Léa Wolff, Falk Butter, Clara Bourbousse, Fredy Barneche, Christophe Tatout, and Aline V. Probst

Supplementary Information

Supplementary Figure 1: *Supplemental information related to* ***Figure 1***

Supplementary Figure 2: *Supplemental information related to* ***Figure 2***

Supplementary Figure 3: *Supplemental information related to* ***Figure 3***

Supplementary Figure 4: *Supplemental information related to* ***Figure 4***

Supplementary Figure 5: *Supplemental information related to* ***Figure 5***

Supplementary Figure 6: *Supplemental information related to* ***Figure 6***

Supplementary Figure 7: *Supplemental information related to* ***Figure 7***

Supplementary Table 1:

1A: Protein sequences of species used in **Figure 1B** and **Supplementary Figure 1A**
1B: Protein sequences of species used in **Figure 1C**

Supplementary Table 2:

2A: DEG in *trb4 trb5* and *trb1 trb2 trb3* mutants (seedlings)
2B: List of genes targeted by TRB4_GFP or TRB1_GFP (seedlings)
2C: List of H3K27me3 and H3K4me3 genes in WT and in *trb4 trb5* mutants (seedlings)
2D: DEG in *trb4-1 trb5-1*, *clf-29* and *trb4-1 trb5-1 clf-29* mutants (leaves)
2E: Z-score values corresponding to Figure 7D
2E: Z-score values corresponding to Figure 7E

Supplementary Table 3:

3A: List of oligos used in this study
3B: List of vectors used in this study
3C: List of antibodies used in this study

Supplementary Table 4: FPKM of PRC1 and PRC2 genes in WT and *trb4 trb5* mutants

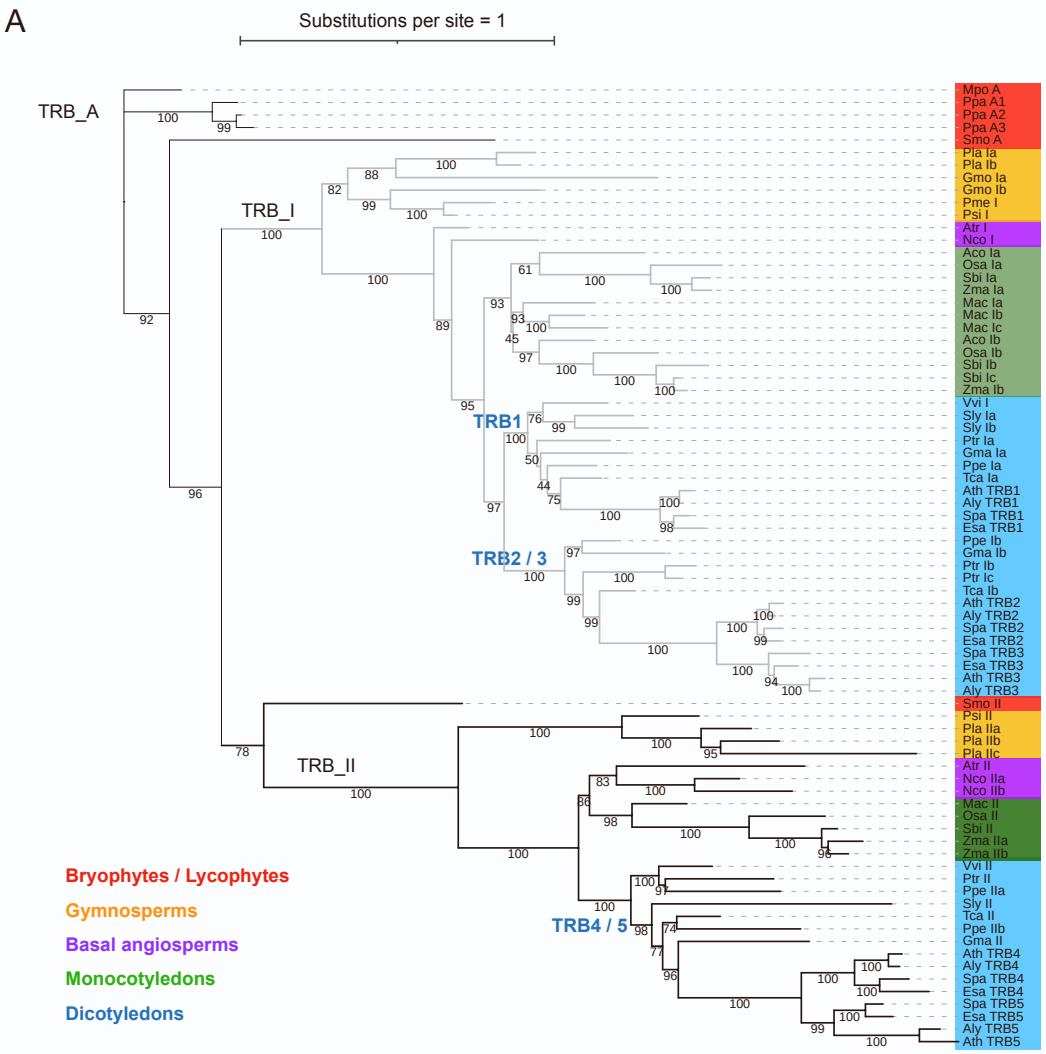
A
Substitutions per site = 1
TRB_A
TRB_I
TRB_II
TRB1
TRB2 / 3
TRB4 / 5
Mpo A
Ppa A1
Ppa A2
Ppa A3
Smo A
Pla Ia
Pla Ib
Gmo Ia
Gmo Ib
Pme I
Psi I
Atr I
Nco I
Aco Ia
Osa Ia
Sbi Ia
Zma Ia
Mac Ia
Mac Ib
Mac Ic
Aco Ib
Osa Ib
Sbi Ib
Sbi Ic
Zma Ib
Vvi I
Sly Ia
Sly Ib
Ptr Ia
Gma Ia
Ppe Ia
Tca Ia
Ath TRB1
Aly TRB1
Spa TRB1
Esa TRB1
Ppe Ib
Gma Ib
Ptr Ib
Ptr Ic
Tca Ib
Ath TRB2
Aly TRB2
Spa TRB2
Esa TRB2
Spa TRB3
Esa TRB3
Ath TRB3
Aly TRB3
Smo II
Psi II
Pla IIa
Pla IIb
Pla IIc
Atr II
Nco IIa
Nco IIb
Mac II
Osa II
Sbi II
Zma IIa
Zma IIb
Vvi II
Ptr II
Ppe IIa
Sly II
Tca II
Ppe IIb
Gma II
Ath TRB4
Aly TRB4
Spa TRB4
Esa TRB4
Spa TRB5
Esa TRB5
Aly TRB5
Ath TRB5
Bryophytes / Lycophytes
Gymnosperms
Basal angiosperms
Monocotyledons
Dicotyledons

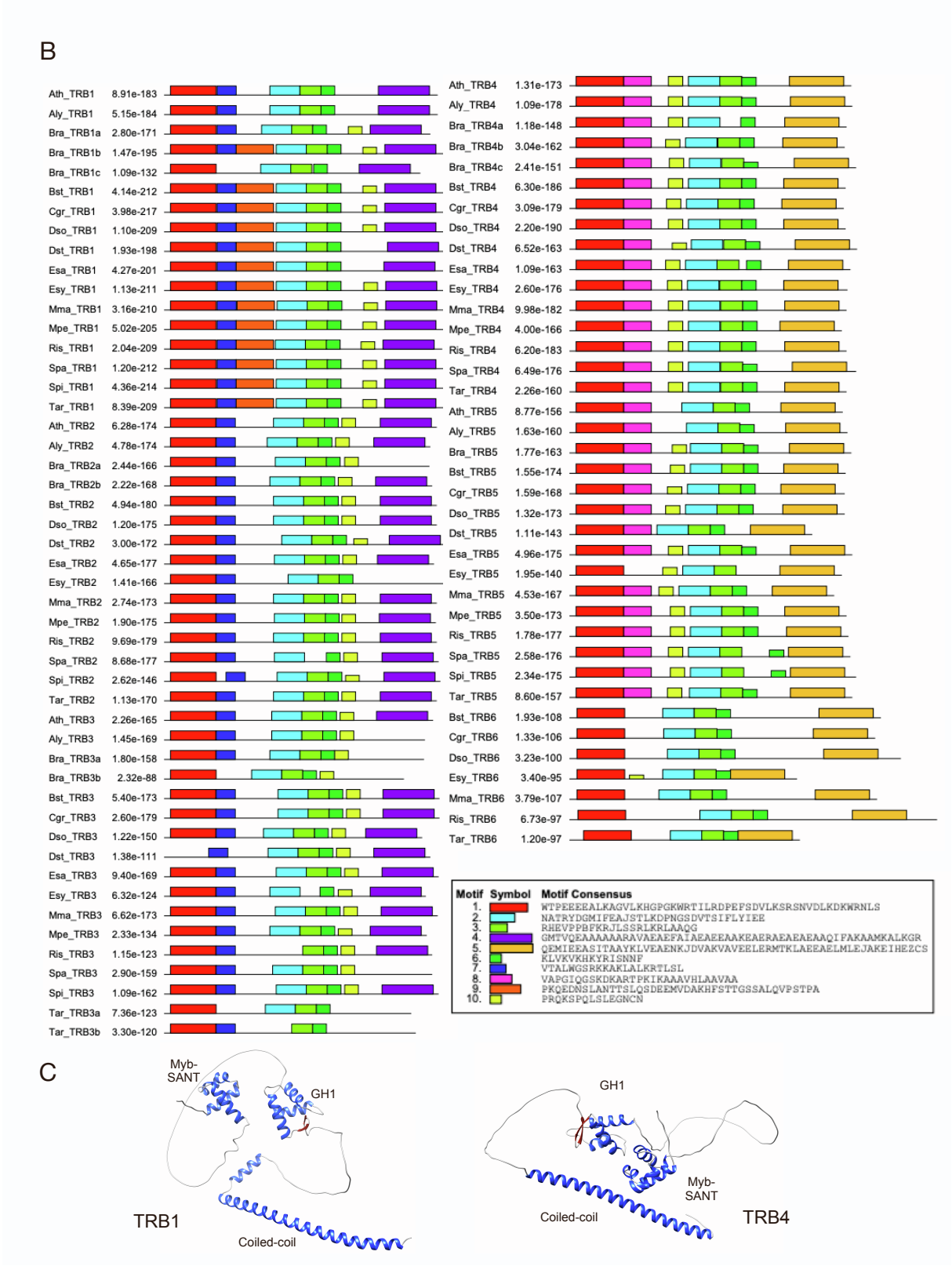

Supplementary Figure 1: *Supplemental information related to Figure 1*

(A) Rooted maximum likelihood phylogenetic tree for TRB orthologs from 24 plant species. Bootstrap values are indicated for each branch. An ancient TRB clade (TRB_A), a clade

comprising Arabidopsis TRB1, TRB2 and TRB3 (TRB_I) and a third clade comprising TRB4 and TRB5 (TRB_II) were defined. **(B)** MEME protein motif prediction of the 10 best motifs among the 15 Brassicaceae species. **(C)** Alpha-fold predictions of long alpha helices in the C-terminal domains of Arabidopsis TRB1 and TRB4 proteins.

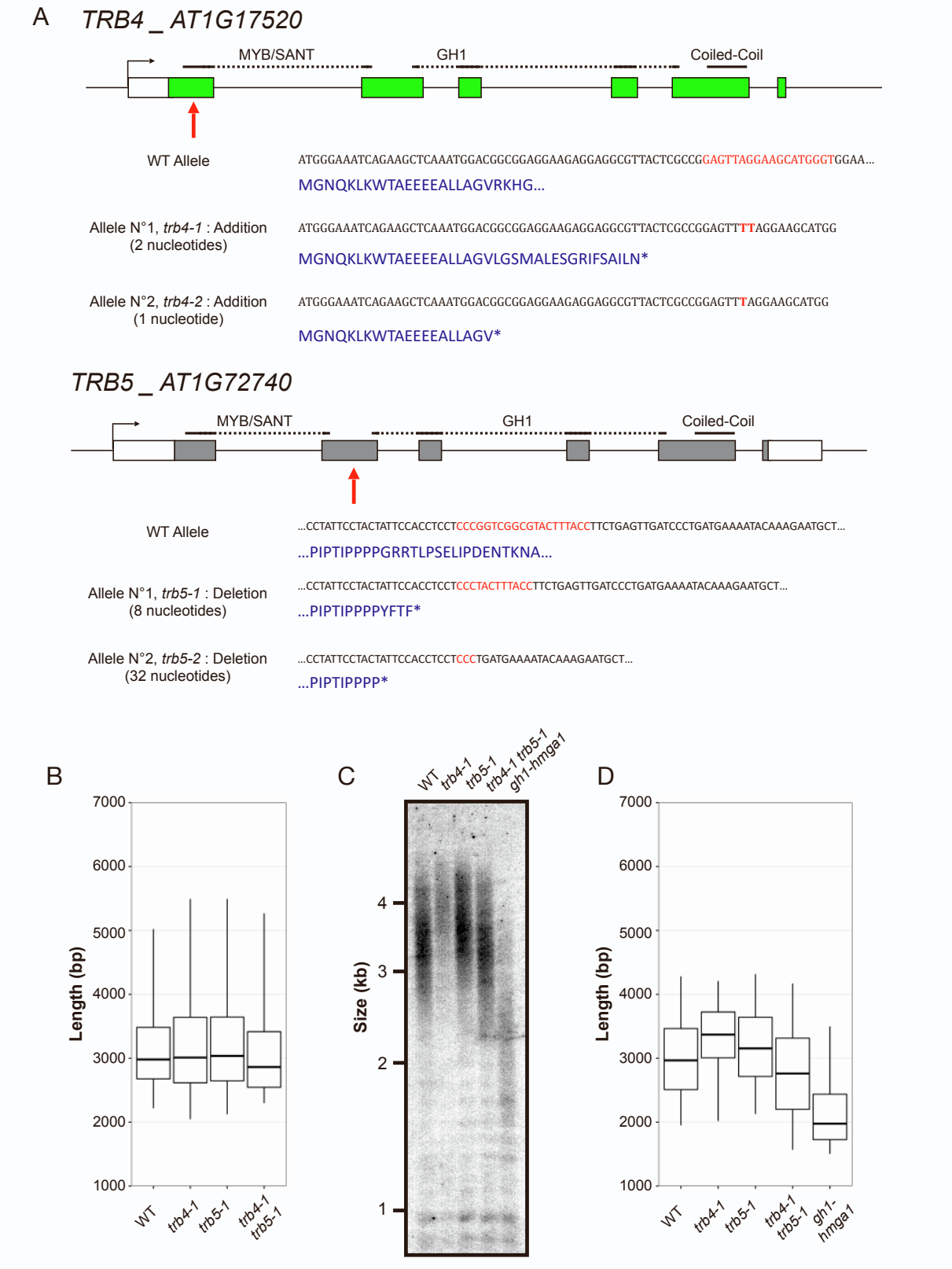
A
TRB4 _ AT1G17520
MYB/SANT
GH1
Coiled-Coil
WT Allele
ATGGGAAATCAGAAGCTCAAATGGACGGCGGAGGAAGAGGAGGCGTTACTCGCCGGAGTTAGGAAGCATGGGTGGAA...
MGNQKLKWTAEEEEALLAGVRKHG...
Allele N°1, trb4-1 : Addition (2 nucleotides)
ATGGGAAATCAGAAGCTCAAATGGACGGCGGAGGAAGAGGAGGCGTTACTCGCCGGAGTTTTAGGAAGCATGG
MGNQKLKWTAEEEEALLAGVLGSMALESGRIFSAILN*
Allele N°2, trb4-2 : Addition (1 nucleotide)
ATGGGAAATCAGAAGCTCAAATGGACGGCGGAGGAAGAGGAGGCGTTACTCGCCGGAGTTTAGGAAGCATGG
MGNQKLKWTAEEEEALLAGV*
TRB5 _ AT1G72740
MYB/SANT
GH1
Coiled-Coil
WT Allele
...CCTATTCCTACTATTCCACCTCCTCCCGGTCGGCGTACTTTACCTTCTGAGTTGATCCCTGATGAAAATACAAAGAATGCT...
...PIPTIPPPPGRRTLPSELIPDENTKNA...
Allele N°1, trb5-1 : Deletion (8 nucleotides)
...CCTATTCCTACTATTCCACCTCCTCCCTACTTTACCTTCTGAGTTGATCCCTGATGAAAATACAAAGAATGCT...
...PIPTIPPPPYFTF*
Allele N°2, trb5-2 : Deletion (32 nucleotides)
...CCTATTCCTACTATTCCACCTCCTCCCTGATGAAAATACAAAGAATGCT...
...PIPTIPPPP*
B
Length (bp)
7000
6000
5000
4000
3000
2000
1000
WT
trb4-1
trb5-1
trb4-1 trb5-1
C
WT
trb4-1
trb5-1
trb4-1 trb5-1
gh1-hmga1
Size (kb)
4
3
2
1
D
Length (bp)
7000
6000
5000
4000
3000
2000
1000
WT
trb4-1
trb5-1
trb4-1 trb5-1
gh1-hmga1

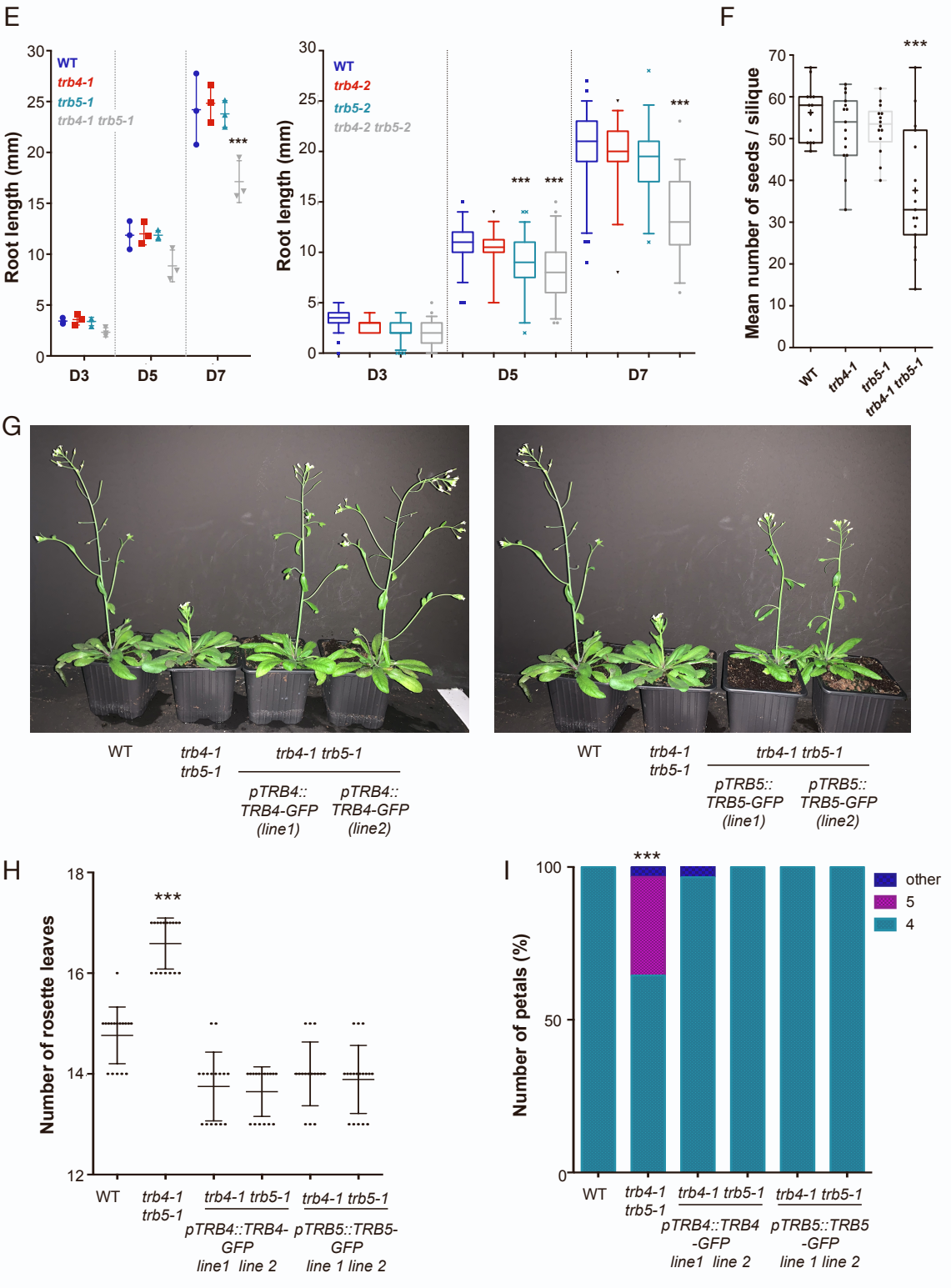
E
WT
trb4-1
trb5-1
trb4-1 trb5-1
Root length (mm)
D3
D5
D7
***
WT
trb4-2
trb5-2
trb4-2 trb5-2
Root length (mm)
D3
D5
D7
***
***
***
F
Mean number of seeds / silique
***
WT
trb4-1
trb5-1
trb4-1 trb5-1
G
WT
trb4-1 trb5-1
trb4-1 trb5-1
pTRB4:: TRB4-GFP (line1)
pTRB4:: TRB4-GFP (line2)
WT
trb4-1 trb5-1
trb4-1 trb5-1
pTRB5:: TRB5-GFP (line1)
pTRB5:: TRB5-GFP (line2)
H
Number of rosette leaves
***
WT
trb4-1 trb5-1
trb4-1 trb5-1
trb4-1 trb5-1
pTRB4::TRB4-GFP line1 line 2
pTRB5::TRB5-GFP line 1 line 2
I
Number of petals (%)
***
other
5
4
WT
trb4-1 trb5-1
trb4-1 trb5-1
trb4-1 trb5-1
pTRB4::TRB4-GFP line1 line 2
pTRB5::TRB5-GFP line 1 line 2

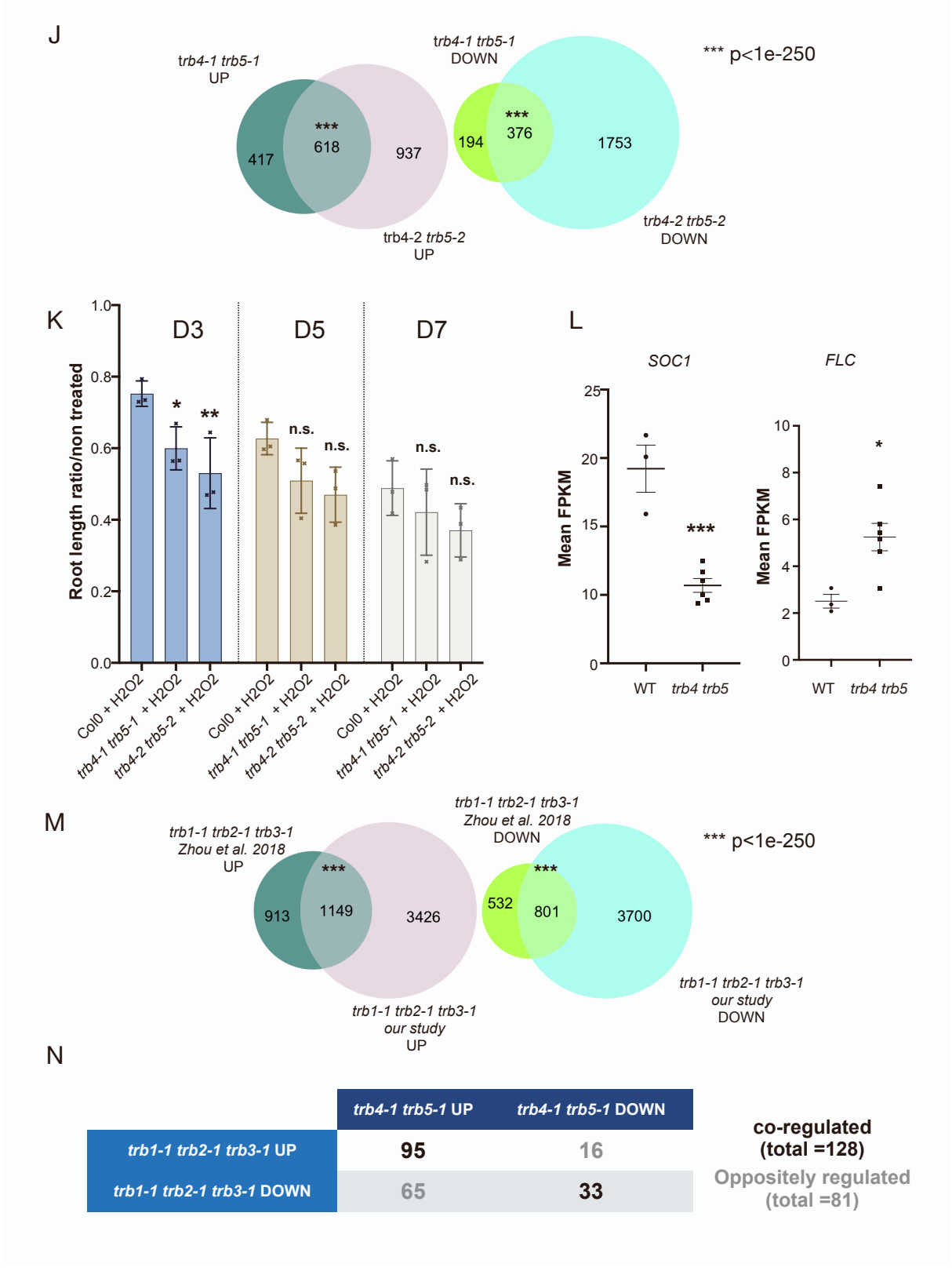

Supplementary Figure 2: *Supplemental information related to Figure 2*

(A) *TRB4* and *TRB5* mutant alleles generated by CRISPR/Cas9. The corresponding nucleotide and the resulting amino acid sequences are shown. In all mutants, premature stop codons are induced. The red arrow indicates the Cas9 target site. **(B)** Telomere Restriction Fragments (TRF) scan analysis from Figure 2C. **(C)** TRF analysis of bulk telomere length in genomic DNA

using telomere repeat probes WT, *trb4-1* and *trb5-1*, *trb4-1 trb5-1* and *gh1-hmga1* mutant. **(D)** TRF scan analysis from panel C. **(E)** Quantification of root length from *in vitro* grown WT, *trb4-1* and *trb5-1* single and *trb4-1 trb5-1* double mutant plantlets (left) and for WT, *trb4-2* and *trb5-2* single and *trb4-2 trb5-2* double mutants (right) at day 3 (D3), 5 (D5) and 7 (D7). For each time point, means from three (left) or two (right) replicates comprising 100 plants each are shown. Roots of *trb4-1 trb5-1 or trb4-2 trb5-2* double mutants are significantly shorter (***p < 0.0001, t-test) at D7. **(F)** Mean number of seeds from 15 siliques of five WT plants, *trb4-1* and *trb5-1* single and *trb4-1 trb5-1* double mutants. Double mutants are significantly less fertile (***p = 0.0004, t-test). **(G)** Representative 4-weeks-old WT, *trb4-1 trb5-1* double mutants and four independent transgenic lines expressing either TRB4-GFP or TRB5-GFP under their respective endogenous promoter. The delayed flowering phenotype of *trb4-1 trb5-1* double mutants is complemented. (**H**) Quantification of leaf number at bolting in WT, *trb4-1 trb5-1* double mutants and four independent transgenic lines shown in (**G**). n = 17, N=1, *** < 0.001, t-test. (**I**) Percentage of flowers showing 4, 5 or any other aberrant petal number in the same genotypes as in (**G**). n=100, N = 5, *** < 0.001, t-test. (**J**) Venn diagram showing up- and down regulated genes relative to WT in RNA-seq analysis from 3 replicates of *trb4-1 trb5-1* and *trb4-2 trb5-2* mutants. FC > 0.5, padj < 0.01. **(K)** Quantification of root length from *in vitro* grown WT, *trb4-1 trb5-1 and trb4-2 trb5-2* double mutant plantlets with or without 2,5mM H_2O_2 at day 3 (D3), 5 and 7. For each time point, the mean ratio of the root length of seedlings grown with or without H_2O_2, from three replicates comprising 50 plants each are shown. Root length development is significantly decreased in presence of H_2O_2 in *trb4-1 trb5-1* or *trb4-2 trb5-2* at D3 (*p < 0.05, **p < 0.005, Anova 2-way). (**L**) Expression level (mean FPKM) of *SOC1* and *FLC* in WT and in *trb4 trb5* mutants. ***<0,0005, *<0,05, t-test (**M**) Venn diagram showing up- and down regulated genes relative to WT in RNA-seq analysis from 3 replicates of *trb1-1 trb2-1 trb3-1* in our data set and the dataset from (Zhou et al., 2018), logFC > 0.5, padj < 0.01. **(N)** Comparison of co- or oppositely regulated genes in *trb4 trb5* and *trb1 trb2 trb3* datasets from (**J**) and (**M**).

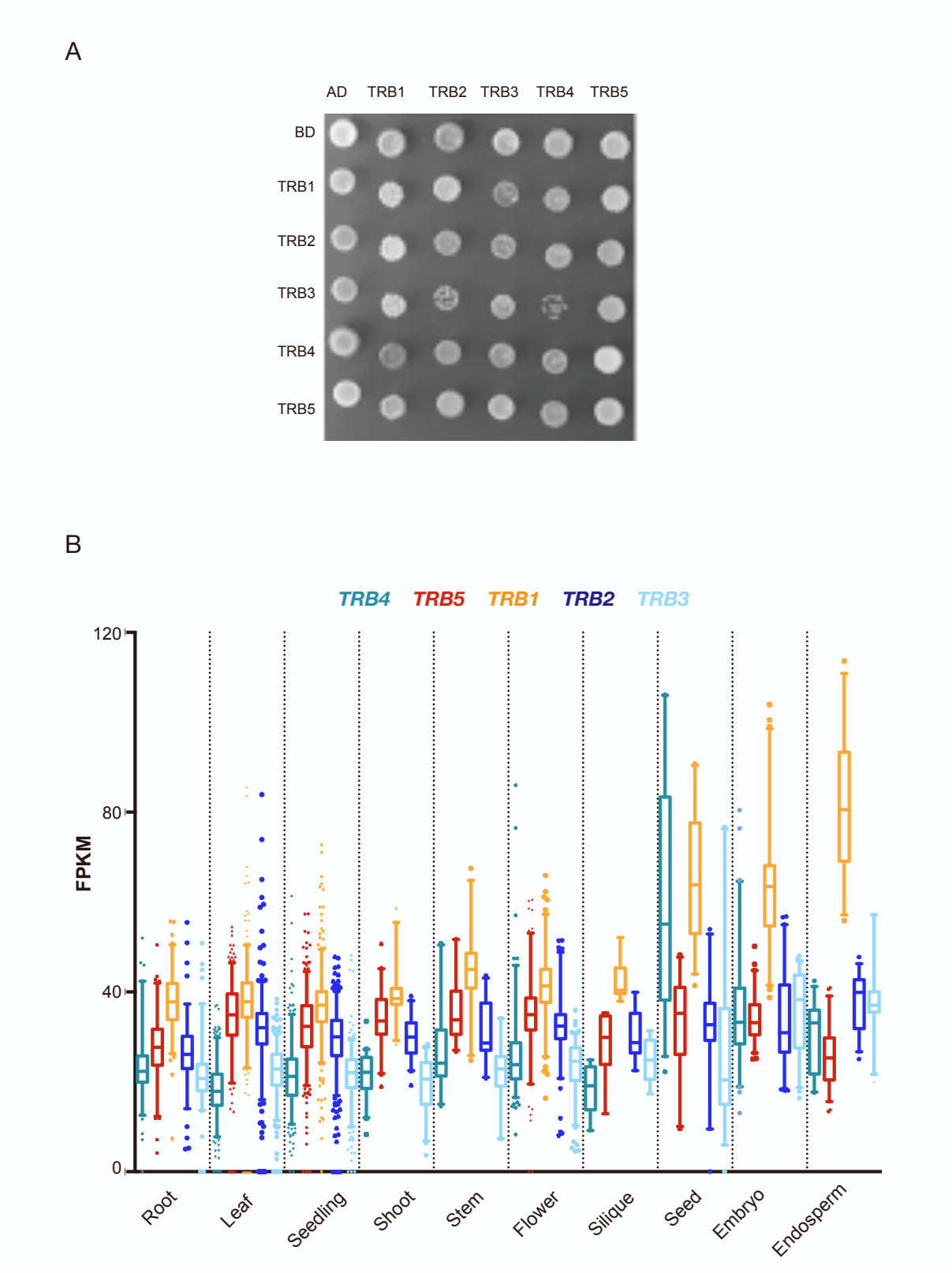

Supplementary Figure 3: *Supplemental information related to Figure 3*

(A) Growth of zygotes on synthetic medium lacking leucine and tryptophan, selecting for the presence of the bait and prey vectors for interactions scored in Figure 3**. (B)** Expression level of *TRB1, TRB2, TRB3, TRB4* and *TRB5* in different Arabidopsis tissues issued from available RNA-seq datasets (data extracted from Arabidopsis RNA-seq Database -

http://ipf.sustech.edu.cn/pub/athrna/). All 5 genes are ubiquitously expressed to similar levels, except in the embryo and endosperm that show higher *TRB1* transcript levels.

A

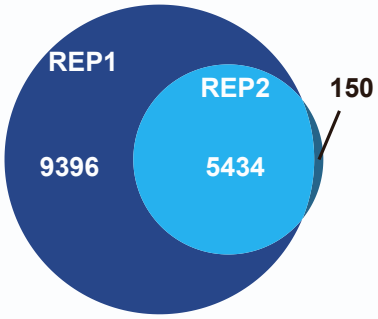

B

Motif	Logo	RC Logo	P-value	E-value	Sites
1-RAAACCCTARW			7.4e-032	1.8e-030	1572 (49.4%)
2-ARGCCCATTW			1.2e-022	2.9e-019	1314 (41.3%)
3-TCGGCCCAA			4.7e-012	1.2e-010	586 (18.4%)
4-GAAGAAGAAGAAG		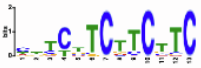	5.7e-010	1.4e-008	939 (29.5%)
5-AAAAAAAAAAAAA	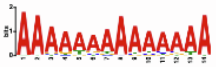	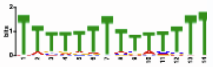	3.4e-007	8.4e-006	309 (9.7%)
6-TATATATA			5.4e-005	1.4e-003	340 (10.7%)

Supplementary Figure 4: *Supplemental information related to Figure 4*

(A) Venn diagram showing overlap between the identified TRB4 targets in the two biological replicates. **(B)** The six most abundant DNA sequence motifs identified by MEME at TRB4 binding sites. Motif 1 corresponds to the telobox, motifs 2 and 3 corresponds to 'site II motif' (*TGGGCY*) (Gaspin et al., 2010).

A

TRB4 cluster1 (5'UTR, n=210)

	Logo	e-value
1		2.0e-242
2	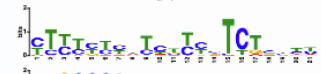	7.1e-054
3	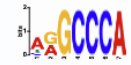	3.3e-020

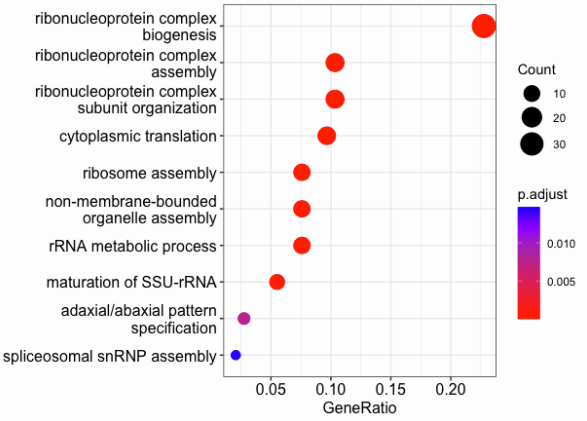

TRB4 cluster2 (5'UTR, n=1646)

	Logo	e-value
1		9.1e-415
2		8.5e-364
3	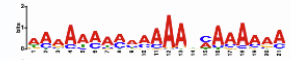	1.2e-033
4		5.8e-030

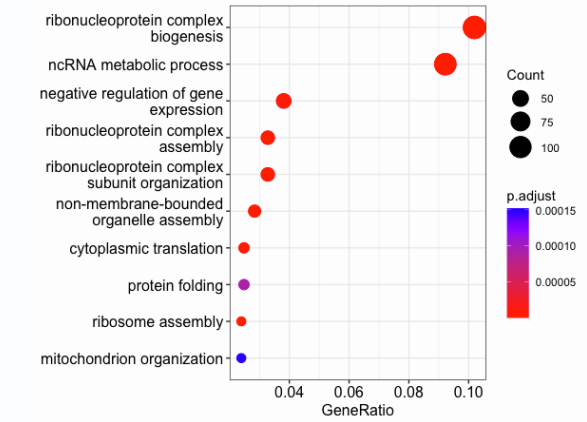

TRB4 cluster3 (promoter, -1000bp, n=3029)

	Logo	e-value
1	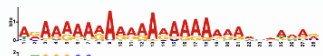	5.4e-088
2		1.7e-014
3	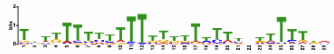	1.8e-014

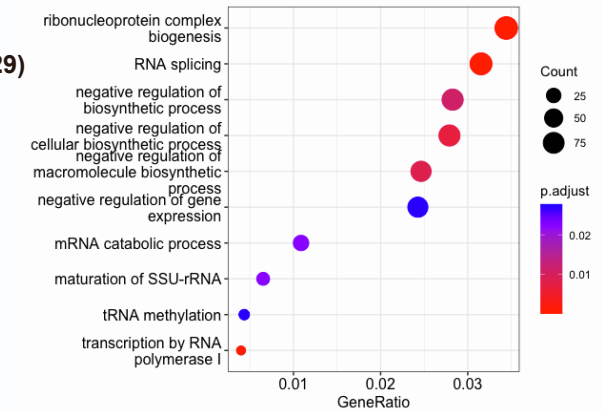

105

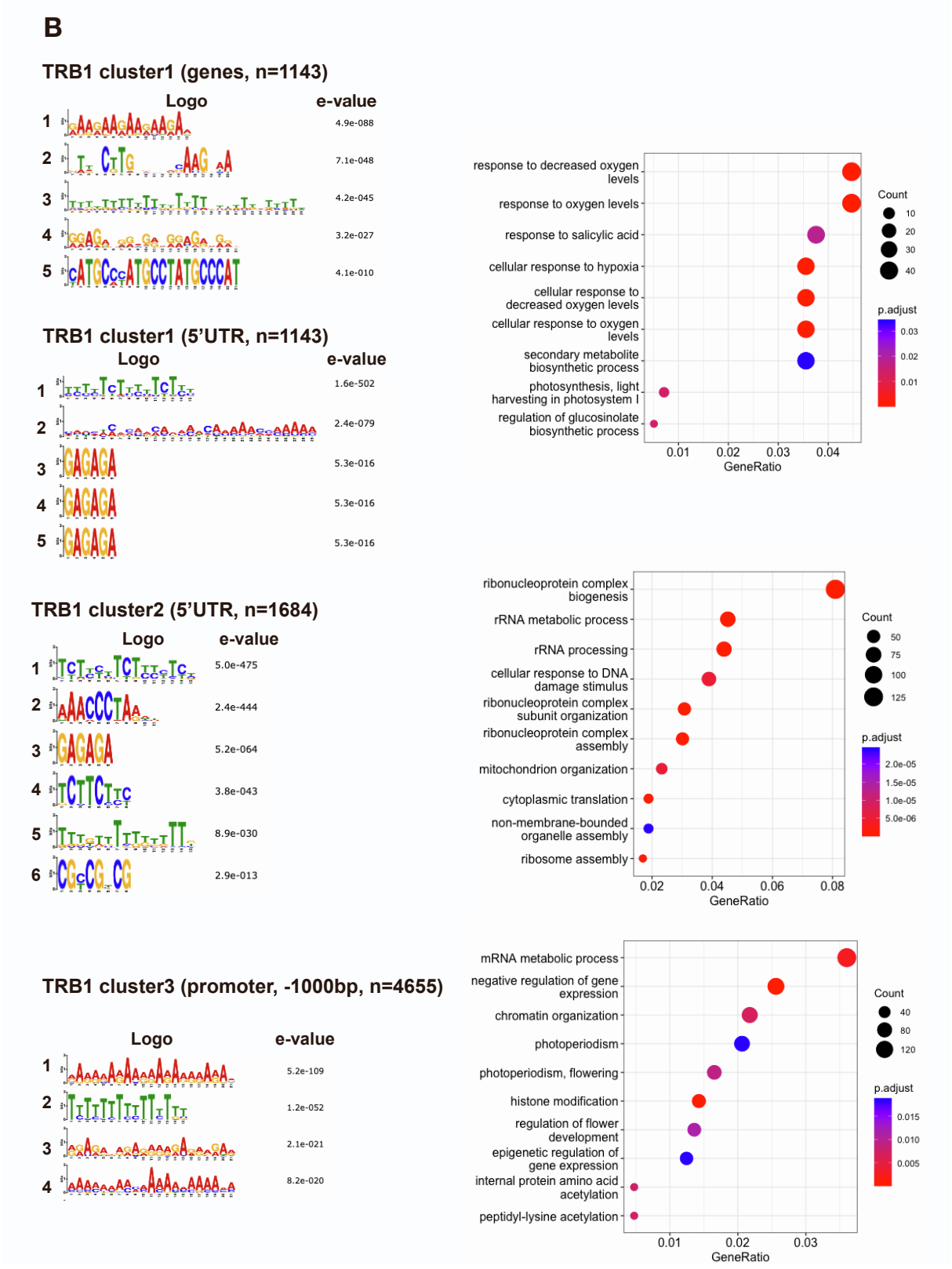

Supplementary Figure 5: *Supplemental information related to Figure 5*

(**A, B**) Left: MEME predictions of up to 6 DNA sequence motifs within the 5'UTR, the promoters (-1000bp from the TTS) of the TRB4 (**A**) or TRB1 (**B**) target genes in the three clusters defined in **Figure 5A-B**. Right: GO-term enrichment of genes corresponding to the three cluster of TRB4 (**A**) and TRB1 (**B**) target genes defined in **Figure 5A-B**.

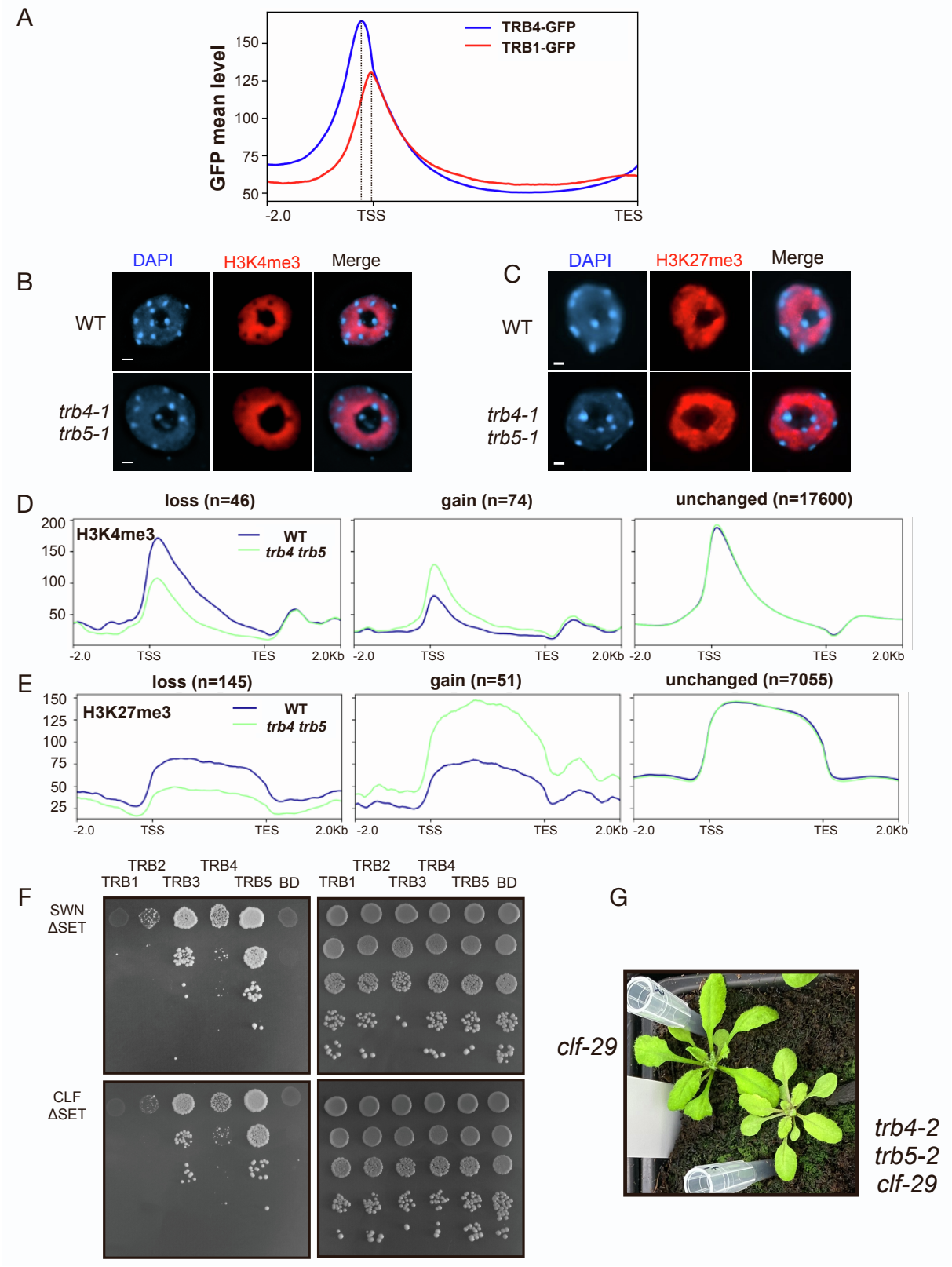

Supplementary Figure 6: *Supplemental information related to Figure 6*

(A) Metagene plot showing ChIP-seq signals of TRB4-GFP or TRB1-GFP over genes enriched in H3K4me3. TRB4 peaks upstream of TRB1. (**B**, **C**) Representative mesophyll leaf nuclei from WT and *trb4-1 trb5-1* mutant plants, immunostained for H3K4me3 **(B)** and H3K27me3

(C). Maximum projections are shown. Scale presents 1 μm. **(D, E)** Metagene plot presentations of H3K4me3 **(D)** and H3K27me3 **(E)** enrichment along genes and 2 kb up and downstream of TSS and TTS with loss, gain or unchanged levels of the histone modifications in *trb4-1 trb5-1* mutants. The number of genes presented in each graph is indicated on the top. (**F**) Y2H serial dilutions examining the interaction of Arabidopsis TRB1 to 5 proteins (as bait) with CURLY LEAF (CLF) and SWINGER (SWN) proteins (lacking the SET domain) (as prey). Left panel: yeast strains growing on synthetic medium lacking Leu, Trp, His and Ade reveal interactions. Right panel: growth of zygotes on synthetic medium lacking Leu and Trp, selecting for the presence of the bait and prey vectors for interactions. Note that the first lines of each panel correspond to the Figure 6C. (G) Representative *clf-29* and *trb4-2 trb5-2 clf-29* triple mutant plants at 3 weeks after sowing.

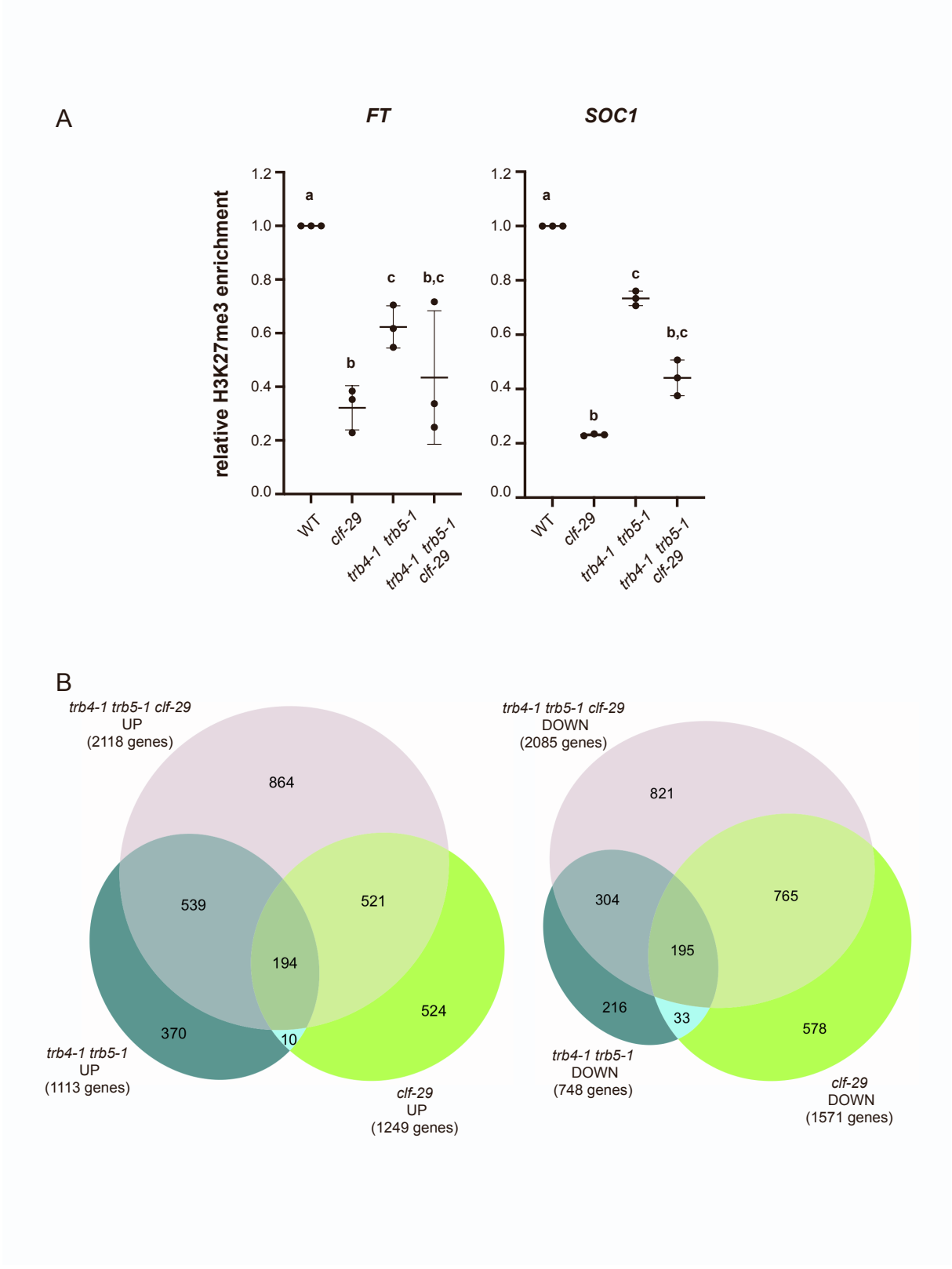

Supplementary Figure 7: *Supplemental information related to Figure 7*

(**A**) Relative enrichment of H3K27me3 normalized to H3 at *FT* and *SOC1* gene promoters in WT, *clf-29*, *trb4-1 trb5-1* and *trb4-1 trb5-1 clf-29* mutants. (**B**) Venn Diagrams showing overlap between up- and down regulated genes in *clf-29*, *trb4-1 trb5-1* and *trb4-1 trb5-1 clf-29* mutants determined by RNA-seq from rosette leaves of 3-week old plants.